Efficient Symbol-Spreading Strategies for Wireless Communication

Gregory W. Wornell

RLE Technical Report No. 587

October 1994

The Research Laboratory of Electronics
MASSACHUSETTS INSTITUTE OF TECHNOLOGY
CAMBRIDGE, MASSACHUSETTS 02139-4307

This work was supported in large part through AT&T Bell Laboratories, Murray Hill, NJ, where the author spent a leave of absence from MIT during the 1992-93 academic year. This work has also been supported in part by the Department of the Navy, Office of the Chief of Naval Research, Grant N00014-93-1-0686 as part of the Advanced Research Projects Agency's RASSP program, and the Air Force Office of Scientific Research under Grant AFOSR-91-0034.

Report Documentation Page

Form Approved
OMB No. 0704-0188

1. REPORT DATE	2. REPORT TYPE	3. DATES COVERED
OCT 1994		**00-10-1994 to 00-10-1994**

4. TITLE AND SUBTITLE	5a. CONTRACT NUMBER
Efficient Symbol-Spreading Strategies for Wireless Communication	5b. GRANT NUMBER
	5c. PROGRAM ELEMENT NUMBER
6. AUTHOR(S)	5d. PROJECT NUMBER
	5e. TASK NUMBER
	5f. WORK UNIT NUMBER
7. PERFORMING ORGANIZATION NAME(S) AND ADDRESS(ES) **Massachusetts Institute of Technology,Research Laboratory of Electronics,77 Massachusetts Avenue,Cambridge,MA,02139-4307**	8. PERFORMING ORGANIZATION REPORT NUMBER
9. SPONSORING/MONITORING AGENCY NAME(S) AND ADDRESS(ES)	10. SPONSOR/MONITOR'S ACRONYM(S)
	11. SPONSOR/MONITOR'S REPORT NUMBER(S)

12. DISTRIBUTION/AVAILABILITY STATEMENT
Approved for public release; distribution unlimited

13. SUPPLEMENTARY NOTES

14. ABSTRACT

15. SUBJECT TERMS

16. SECURITY CLASSIFICATION OF:			17. LIMITATION OF ABSTRACT	18. NUMBER OF PAGES	19a. NAME OF RESPONSIBLE PERSON
a. REPORT	b. ABSTRACT	c. THIS PAGE			
unclassified	**unclassified**	**unclassified**		**82**	

Standard Form 298 (Rev. 8-98)
Prescribed by ANSI Std Z39-18

Abstract

Some efficient new classes of algorithms for compensating for fading in wireless systems are introduced. For single-user or frequency-division multiplexed wireless systems, we develop a technique we refer to as spread-response precoding which replaces the interleaver traditionally used in conjunction with coding in such systems. From the perspective of the coded symbol stream, spread-response precoding effectively transforms an arbitrary Rayleigh fading channel into a nonfading, simple white marginally Gaussian noise channel with no intersymbol interference. Furthermore, spread-response precoding requires no additional power or bandwidth, and is attractive in terms of computational complexity, robustness, and delay considerations.

In the multiuser case, spread-response precoding generalizes to a new class of orthogonal code-division multiple-access (CDMA) systems for efficient communication in environments subject to multipath fading phenomena. The key characteristic of these new systems, which we refer to as "spread-signature CDMA" systems, is that the associated signature sequences are significantly longer than the interval between symbols. Using this approach, the transmission of each symbol of each user is, in effect, spread over a wide temporal and spectral extent, which is efficiently exploited to combat the effects of fading.

Both efficient signature sets and efficient receiver structures for such systems are developed. Several aspects of the performance of the resulting spread-signature CDMA systems are presented, including both the achievable bit error rate characteristics as well as the effective capacity of such systems. The results suggest that spread-signature CDMA may be an attractive alternative to conventional CDMA in a variety of application scenarios.

Acknowledgements

This work was supported in large part through AT&T Bell Laboratories, Murray Hill, NJ, where the author spent a leave of absence from MIT during the 1992-93 Academic Year. This work has also been supported in part by the Advanced Research Projects Agency monitored by ONR under Contract No. N00014-93-1-0686, and the Air Force Office of Scientific Research under Grant No. AFOSR-91-0034.

The author thanks N. S. Jayant, C-E. Sundberg, N. Seshadri, J. Kovacevic, M. Sondhi, A. Odlyzko, E. Teletar, A. Wyner, and S. Shamai (Shitz), all at AT&T Bell Laboratories, for many engaging discussions, insightful comments and helpful suggestions in the course of this work.

Contents

List of Figures

Part I

Spread-Response Precoding

I.1 Introduction

The need to reliably transmit analog and digital data over channels subject to fading arises in a wide range of applications including mobile radio and personal wireless systems, and audio and television broadcasting. Generally, the fading characteristics of the channel, which are a function of both the nature of the transmission media and the relative motions of the transmitter and receiver in a given system, lead to variations in the quality of channel both in time and in frequency.

Diversity techniques are widely used in communication systems to compensate for these variations [1] [2]. These range from simple multiple transmission strategies in time, frequency, and space, to more sophisticated diversity techniques based on the use of coding. In such scenarios, coding is used to combat both the effects of fading and the effects of stationary additive noise.

In order for coding to be effective against fading in particular, it is generally necessary to combine coding with interleaving, a simple but nevertheless useful form of precoding. The purpose of interleaving is to scramble the coded data stream so that fading channel effectively seen by this stream is uncorrelated from time-sample to time-sample. This substantially reduces the coding complexity required to achieve a given level of fidelity, allowing shorter lengths in the case of block codes, or fewer states in the case of convolutional codes.

In this part of the report, we develop an attractive alternative to interleaving which we term "spread-response precoding." With spread-response precoding, the fading channel as seen by the coded data stream is effectively transformed into a simple additive white noise channel. As a result, when combined with coding techniques such as trellis-coded modulation, the precoding stage combats any fading effects, while the coding stage combats the remaining additive noise. This partitioning appears to be rather attractive in terms of system complexity considerations. Indeed, spread-response precoding, in requiring comparatively simple linear signal processing at transmitter and receiver, is significantly less demanding computationally than error-correcting coding and decoding algorithms. Moreover, precoding constitutes a diversity strategy that incurs no additional cost in terms of bandwidth or power, and is competitive with traditional approaches in terms of robustness and delay considerations.

While it has generally been understood in the communications community that inter-

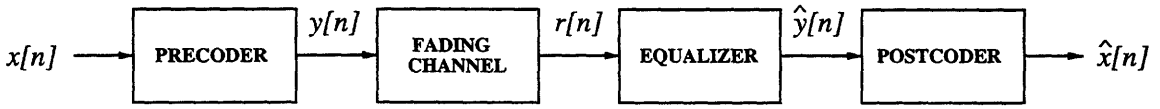

Figure I.1: *Precoding system.*

leaving is not generally the most efficient of precoding strategies (see, *e.g.*, [3]), the literature has offered surprisingly few alternatives to date. Perhaps the work closest in spirit to the ideas presented here is contained in [4], although in this case the author developed a form of precoding for use *in conjunction* with interleaving rather than as an alternative to interleaving.

This part of the report is organized as follows. In Section I.2, we outline the Rayleigh fading channel model we consider. In Section I.3, we develop the transmitter portion of the system, and discuss fundamental design and implementation tradeoffs. In Section I.4, we turn our attention to the receiver portion of the system, developing optimum designs. In Section I.5, we explore aspects of the performance of systems using precoding, including theoretical capacity and attainable bit error rate calculations. Finally, Section I.6 contains some concluding remarks.

I.2 System Model

Fig. I.1 depicts a block diagram of the overall system we consider. In this figure, $x[n]$ is the complex-valued M-ary symbol sequence representing the coded bit stream, and $y[n]$ is the precoded symbol stream to be transmitted. The transmitted data $y[n]$ is corrupted by complex-valued fading and additive noise, producing $r[n]$ at the receiver. The received data is first processed by an equalizer to produce $\hat{y}[n]$, then by a postcoder to produce $\hat{x}[n]$. Finally, a decoder (not shown) processes $\hat{x}[n]$ to produce an estimate of the original bit stream.

The channel in Fig. I.1 is the equivalent discrete-time baseband model of a fairly general stationary Rayleigh fading channel with uncorrelated scattering and bandwidth $\mathcal{W}_0$. The channel consists of two components, a linear time-varying filter which captures the effects of multipath fading due to multiple scatters in the transmission medium, and an additive noise term representing both receiver noise and, more significantly, co-channel interference.

More specifically, the response of the channel to an input sequence $y[n]$ is given by

$$r[n] = \sum_k a[n;k]\, y[n-k] + w[n] \tag{I.1}$$

where $w[n]$ is a zero-mean complex stationary white Gaussian sequence with variance

$$E\left[|w[n]|^2\right] = \mathcal{N}_0\mathcal{W}_0,$$

and $a[n;k]$, the response of the channel at time n to a unit-sample at time $n-k$, is a complex Gaussian fading process. For fixed values of k, the $a[n;k]$ are zero-mean complex jointly stationary and Gaussian sequences. Furthermore, uncorrelated scattering implies

sequences corresponding to distinct values of k are statistically independent. Hence,

$$E\left[a[n;k]\,a^*[n-m;l]\right] = R_a[m;k]\,\delta[k-l]$$

where $\delta[n]$ is the unit-sample, *i.e.*,

$$\delta[n] \triangleq \begin{cases} 1 & n=0 \\ 0 & \text{otherwise} \end{cases}. \tag{I.2}$$

With uncorrelated scattering, the time-variant channel frequency response[1]

$$A(\omega;n] = \sum_k a[n;k]\,e^{-j\omega k} \tag{I.3}$$

is then stationary in both n and ω and satisfies

$$E\left[A(\omega;n]\right] = 0 \tag{I.4a}$$

$$E\left[|A(\omega;n]|^2\right] = \sigma_a^2. \tag{I.4b}$$

Both $w[n]$ and $a[n;k]$ are assumed to be statistically independent of the input to the channel.

Finally, we assume that while the transmitter does not have access to the fading channel kernel $a[n;k]$ or its statistics, these parameters are known, or, more typically, can be reliably measured at the receiver.

I.3 Spread-Response Precoding

In this section, we consider, specifically, the transmitter portion of the system in Fig. I.1. We begin by observing that although the detailed characteristics of a fading channel fluctuate from time sample to time sample, the performance of communication systems using such channels is generally dictated by the *average* characteristics of that channel over time. Certainly most capacity estimates for such channels involve averaging of this type; see, *e.g.*, [5] and the references therein. As a consequence, in principle an efficient communication strategy for such channels would, in some sense, "spread" the transmission of each symbol over a large number of time samples.

Conveniently, spreading of this type can be achieved through simple linear time-invariant (LTI) filtering of the coded symbol stream—a form of precoding. Specifically, denoting the unit-sample response of the precoding filter by $h[n]$, the transmitted sequence is[2] (*cf.* Fig. I.1)

$$y[n] = x[n] * h[n] = \sum_k x[k]\,h[n-k]. \tag{I.5}$$

[1]We adopt the useful convention of using parentheses $(\cdot)$ to denote continuous-valued arguments and brackets $[\cdot]$ to denote discrete-valued arguments. For functions of two arguments where the first is continuous and the second is discrete (as in the case of time-variant frequency responses) we use the convenient mixed notation $(\cdot;\cdot]$. The notation $[\cdot;\cdot)$ is used in a similar manner.

[2]We use operator $*$ to denote convolution, and the superscript * to denote complex conjugation.

For convenience, we restrict our attention to the case in which $h[n]$ is a real-valued sequence.

It is also highly desirable for the precoding to be lossless, in which case $y[n]$ constitutes an orthonormal transformation of the data symbols $x[n]$. Lossless LTI filters satisfy the time-domain constraint

$$\sum_n h[n-k]\,h[n-l] = \delta[k-l]. \tag{I.6}$$

In the frequency domain, the condition (I.6) corresponds to

$$|H(\omega)|^2 = 1, \tag{I.7}$$

and, for this reason, lossless filters are frequently referred to as *allpass* filters in the signal processing literature [6]. An important property of such filters which follows immediately from (I.6) is that

$$h^{-1}[n] = h[-n].$$

Accordingly, we may conveniently and stably recompute $x[n]$ from $y[n]$ according to

$$x[n] = y[n] * h[-n] = \sum_k y[k]\,h[k-n]. \tag{I.8}$$

From a practical standpoint, it is generally necessary to restrict our attention to finite impulse response (FIR) precoders. However, as is well known, the only lossless FIR filters are the shifted unit-samples, *i.e.*, $h[n] = \delta[n-k]$ for arbitrary k. Nevertheless, many infinite impulse response (IIR) lossless filters have strongly localized temporal support and can be therefore be truncated without significantly altering their characteristics. More generally, there are a wide variety of FIR filters that closely approximate the losslessness condition (I.6).

To make this notion of approximation more precise, consider the class of LTI filters $h[n]$ with unit-energy, *i.e.*,

$$\sum_n h^2[n] = 1, \tag{I.9}$$

and let

$$\Phi_h[n] = h[n] * h[-n] = \sum_k h[k]\,h[k-n]$$

denote the autocorrelation function. Then, since the autocorrelation of a perfectly lossless filter is the unit-sample, a useful measure of the deviation from losslessness is the reciprocal of the total sidelobe energy in the autocorrelation function. Specifically, we may define the following convenient losslessness merit factor $\mathcal{L}^h$ for a unit-energy filter $h[n]$:

$$\mathcal{L}^h = \left(\sum_n (\Phi_h[n] - \delta[n])^2\right)^{-1} = \left(2\sum_{n=1}^{\infty} \Phi_h^2[n]\right)^{-1} \tag{I.10}$$

with large $\mathcal{L}^h$ corresponding to filters that are nearly lossless. More specifically, we have $0 < \mathcal{L}^h \leq \infty$ with the right-hand equality if and only if the filter is perfectly lossless. This merit factor is, in fact, identical to that introduced by Golay to evaluate the quality of low autocorrelation binary sequences [7], and we note that it is sometimes useful to exploit an

equivalent frequency-domain definition for $\mathcal{L}^h$, *viz.*,

$$\mathcal{L}^h = \left(\frac{1}{2\pi} \int_{-\pi}^{\pi} \left(|H(\omega)|^2 - 1 \right)^2 d\omega \right)^{-1},$$

which can be verified by applying Parseval's theorem to (I.10).

While losslessness is an important attribute of a precoding filter, a second important attribute concerns their effectiveness in their primary function: spreading the transmission of each symbol over a large number of time samples. This is achieved when the precoder's unit-sample response energy is widely dispersed in time, or, equivalently, when the precoding system has strong partial response characteristics. Indeed, one can interpret spread-response precoding as a form of partial-response precoding, although the objectives of traditional partial-response precoding are markedly different.

A useful measure of dispersion for an arbitrary unit-energy filter $h[n]$ in the context of this work is given by

$$\mathcal{D}_h = \left(\sum_n h^4[n] \right)^{-1} \tag{I.11}$$

with large $\mathcal{D}_h$ corresponding to good spreading characteristics. Using (I.9), it follows that for unit-energy filters

$$\mathcal{D}_h \geq 1 \tag{I.12}$$

with equality when $h[n] = \delta[n]$. However, for FIR filters of length N with unit-energy, (I.9) also implies that

$$\mathcal{D}_h \leq N$$

with equality precisely when

$$|h[n]| = 1/\sqrt{N}, \quad \text{all } 0 \leq n \leq N-1.$$

Consequently, for FIR precoders maximum dispersion (*i.e.*, $\mathcal{D}_h = N$) is obtained when $h[n]$ is an antipodal (binary) sequence. Conveniently, binary sequences are also highly attractive in terms of both computational efficiency and numerical sensitivity.

While both good losslessness and spreading characteristics are desirable in design of FIR precoders, they are competing objectives. Based on the preceding discussion, at one extreme the precoder $h[n] = \delta[n]$ corresponds to the best possible $\mathcal{L}^h$ but the worst possible $\mathcal{D}_h$. At the opposite extreme, precoders with binary-valued unit-sample responses provide the best possible $\mathcal{D}_h$ for a given length constraint, but poor values of $\mathcal{L}^h$. Indeed, a conjecture of Golay [8] based on an ergodicity postulate suggests that for such binary sequences

$$\max_h \mathcal{L}^h \to 12.3247\cdots \quad \text{as } N \to \infty.$$

Consequently, as we will discuss later, for a fixed filter length prescribed by external delay constraints imposed on the overall system, the precoder design process requires a compromise between the two components.[3]

[3]Actually, as we'll discuss in Section II.5.1, this problem can be circumvented by using only a slightly more

When spread-response precoding is used in a system, the transmitted data have some rather special asymptotic characteristics. First, we note that with lossless precoding we get, via (I.7), that the transmitted stream $y[n]$ will have same power spectrum as the original coded data $x[n]$, *i.e.*,

$$S_y(\omega) = S_x(\omega).$$

In particular, when $x[n]$ is a sequence of statistically independent complex-valued symbols each with energy $\mathcal{E}_s$, then $y[n]$ is a complex wide-sense stationary white sequence with variance $\mathcal{E}_s$. In addition, it can be shown that in the limit of infinite dispersion ($\mathcal{D}_h \to \infty$) the transmitted stream is marginally Gaussian, *i.e.*, that each transmitted sample $y[n]$ has a Gaussian distribution. This follows from a straightforward Central Limit Theorem argument: using (I.5) we see each $y[n]$ is the balanced sum of a large number of independent random variables. From the point of view of transmission security and capacity considerations, such characteristics are rather appealing. However, we should also note that from the point of view of peak-to-average power and receiver synchronization requirements, these characteristics present important practical challenges in terms of system design. However, such considerations are beyond the scope of the present report.

I.3.1 Precoder Design

As will become apparent, the overall system performance depends in a rather complicated manner on the loss and dispersion characteristics of the precoding filter. Furthermore, even if a weighted combination of the losslessness and dispersion factors were to correspond to some reasonable measure of ultimate system performance, optimizing such a criterion is an intrinsically difficult numerical problem.

Nevertheless, there are a number of approaches that work well in practice for obtaining precoding filters corresponding to a reasonable compromise between losslessness and dispersion factors, and providing good overall system performance. In fact, design techniques are suggested from a variety of sources, largely because such filters find application in a number of distinct communication problems ranging from the mitigation of impulse noise in communication systems [9] to robust quantization of non-Gaussian sources [10]. Those we discuss here are closely related to the techniques which have proven useful in these problems.

As discussed earlier, binary precoders have attractive computational properties and optimal dispersion factors but poor losslessness factors. The binary sequences having optimal losslessness factors for a given length constraint N are tabulated[4] in [11] for $N \leq 71$. For length $N = 13$, the corresponding sequence is, for example, the well-known Barker sequence for which $\mathcal{L}^h \approx 14.08$. Likewise, for length $N = 27$, the optimum sequence has $\mathcal{L}^h \approx 9.85$. Another class of binary sequences with better-than-average losslessness characteristics are the maximal length shift register sequences (or m-sequences) [12], for which $\mathcal{L}^h \sim 3$ for large N as shown in [13].

---

complicated linear precoder structure—in particular, one that is not time-invariant but rather periodically time-varying.

[4]Actually, to simplify the search for such sequences, typically only skew-symmetric binary sequences are considered. This restriction is not severe however, since this class generally includes many of the best sequences even when the restriction is removed.

In practice, the losslessness characteristics of these sequences can be markedly improved while largely preserving their dispersion properties by relaxing their binary amplitude constraints in a controlled manner. One way to accomplish this is to apply the following simple heuristic algorithm. Beginning with an initial binary sequence $h_0[n]$, we proceed to maximize $\mathcal{L}^h$ in the form (I.10) via an iterative ascent algorithm (such as the Simplex method) subject to the unit-energy constraint (I.9). Naturally, a global optimization would result in the trivial solution $\delta[n]$. However, the objective function typically has many local maxima, and in practice, the algorithm generally converges to such a fixed point, and results in a filter with substantially improved $\mathcal{L}^h$ at a relatively modest cost in $\mathcal{D}_h$.

Other filters with reasonable dispersion factors are also suitable as an initialization for this type of algorithm. For instance, in [10] a chirp sequence of the form

$$h_0[n] = \beta \sin\left[\frac{\pi n(n-1)}{2N}\right], \quad \text{for } n = 0, 1, \ldots, N-1$$

is used with good results. This initialization is especially useful in the design of very long precoders, in which case the corresponding optimal binary sequences are unknown. However, depending on the specific value of N and on the specific iterative descent algorithm, certain initializations lead to better precoders than others in terms of overall system performance. Consequently, trial and error is invariably involved.

I.4 System Characteristics and Receiver Design

In this section, we turn our attention to the receiver portion of the system in Fig. I.1. We begin by noting that the receiver for decoding the bit stream can be partitioned into two stages. The first is the equalization stage, which, as depicted in Fig. I.1 and without loss of generality, can be described as the cascade of an equalizer and postcoder. The second is the decoding stage (not shown in Fig. I.1), typically consists of some form of Maximum Likelihood (ML) sequence detection. As will become apparent, when no coding is employed, simple symbol-by-symbol detection generally suffices at the decoder. However, in the sequel we restrict our attention to the equalization and postcoding stages.

In general, the equalizer, which compensates for the fading, is a linear time-varying filter whose kernel is $b[n;k]$, so that

$$\hat{y}[n] = \sum_k b[n;k]\, r[n-k].$$

Typically, this kernel is a function of the fading channel kernel $a[n;k]$ and the noise statistics, both of which are assumed to be available at the receiver.

In turn, the postcoder inverts the transformation of input symbols that takes place during precoding, and is simply a linear filter whose unit-sample response is (*cf.* (I.8)) a time-reversed version of the lossless precoding filter $h[n]$, *i.e.*,

$$\hat{x}[n] = h[-n] * \hat{y}[n]. \tag{I.13}$$

The overall system consisting of the channel with precoding, equalization, and post-

coding, we refer to, for convenience, as the "composite channel." In the remainder of this section we first derive the key properties of this composite channel, then optimize them through judicious choice of the equalizer parameters.

Our main result is that subject to only relatively mild ergodicity constraints on channel the use of lossless precoding with a large dispersion factor leads asymptotically to an additive white noise composite channel that is not only free of fading, but has no intersymbol interference. In order to make our result precise, we first define a sufficiently realistic class of ergodic kernels for our purposes, which, for convenience, we term "admissibly ergodic."

Definition 1 *Let $f[n;k]$ be the kernel of a linear system, and define*

$$\tilde{f}[n;k] = f[n;k] - E\left[f[n;k]\right]. \tag{I.14}$$

Furthermore, let

$$d[n;k] = \sum_l \tilde{f}[n;l]\,\tilde{f}^*[n-k;l-k] \tag{I.15}$$

and define

$$\tilde{d}[n;k] = d[n;k] - E\left[d[n;k]\right]. \tag{I.16}$$

Then $f[n;k]$ is an admissibly ergodic *kernel if the following conditions are satisfied:*

$$E\left[f[n;k]\right] = \mu\,\delta[k] \quad \textit{for every } k,n \tag{I.17a}$$

$$E\left[\tilde{f}[n;k]\,\tilde{f}^*[n-m;l]\right] = R[m;k]\,\delta[k-l] \quad \textit{for every } k,l,m,n \tag{I.17b}$$

$$E\left[\tilde{d}[n;k]\,\tilde{d}^*[n-m;l]\right] = T[m;k,l] \quad \textit{for every } k,l,n,m \tag{I.17c}$$

$$S_R = \sum_k \sum_n |R[n;k]| < \infty \tag{I.17d}$$

$$S_T = \sum_{k,l} \sum_m |T[m;k,l]| < \infty. \tag{I.17e}$$

Before proceeding, we adopt some convenient nomenclature. In general it will be convenient to view a generic linear kernel such as $f[n;k]$ as a collection of sequences in n indexed by k. Hence, when we refer to "the sequence $f[n;k]$" we specifically mean the sequence in n corresponding to a fixed (but generally arbitrary) value of k. From this viewpoint, the conditions in Definition 1 are straightforward to interpret. Conditions (I.17a), (I.17b), and (I.17c) are essentially stationarity constraints. They ensure, specifically, that the kernel sequences $f[n;k]$ and the correlation sequences $d[n;k]$ are each jointly wide-sense stationary. The condition (I.17b) also ensures that sequences $f[n;k]$ corresponding to distinct values of k are uncorrelated. Finally, conditions (I.17d) and (I.17e) in effect ensure that linear combinations of the kernel sequences $f[n;k]$ are mean- and correlation-ergodic.

Equivalently, the conditions in Definition 1 can be interpreted in terms of stationarity and ergodicity constraints on the time-variant system frequency response

$$F(\omega;n] = \sum_k f[n;k]\,e^{-j\omega k}. \tag{I.18}$$

We note, in particular, that (I.17a) and (I.17b) imply that $F(\omega;n]$ is wide sense-stationary

in both n and ω and satisfies

$$E\left[F(\omega;n]\right] = \mu. \tag{I.19}$$

Furthermore, with

$$\tilde{F}(\omega;n] = F(\omega;n] - E\left[F(\omega;n]\right]$$

we have

$$E\left[\tilde{F}(\theta;n]\,\tilde{F}^*(\theta-\omega;n-m]\right] = \Psi(\omega;m], \tag{I.20}$$

where $\Psi(\omega;m]$ is the spaced-frequency spaced-time correlation function of the system and satisfies

$$\Psi(\omega;m] = \sum_k R[m;k]\,e^{-j\omega k}. \tag{I.21}$$

Finally, for completeness, we note that

$$S(\lambda;k] = \sum_m R[m;k]\,e^{-j\lambda m} \tag{I.22}$$

is the system's scattering function,

$$\Upsilon(\lambda) = \sum_m \Psi(0;m]\,e^{j\lambda m} \tag{I.23}$$

is the system's Doppler power spectrum, and

$$\sigma_k^2 = R[0;k] = \mathrm{var}\, f[n;k] \tag{I.24}$$

is the multipath intensity profile or delay power spectrum of the system. Hence, the total power is given by

$$\sigma^2 \triangleq \mathrm{var}\left[F(\omega;n]\right] = \Psi(0;0] = \sum_k \sigma_k^2. \tag{I.25}$$

We can now present our main theorem concerning the composite system depicted in Fig. I.1. A proof is presented in Appendix III.A.

Theorem 1 *Let $x[n]$ be a sequence of zero-mean, uncorrelated symbols, each with energy $\mathcal{E}_s$; let $a[n;k]$ and $w[n]$ be as defined in (I.1); and let $c[n;k]$ denote the kernel of the composite linear system formed by cascading the channel corresponding to kernel $a[n;k]$ with the equalizer corresponding to kernel $b[n;k]$, i.e.,*

$$c[n;k] = \sum_l b[n;l]\,a[n-l;k-l]. \tag{I.26}$$

Finally, suppose $c[n;k]$ and $b[n;k]$ are both admissibly ergodic kernels in the sense of Definition 1. Then, as $\mathcal{D}_h \to \infty$, we have[5], for each n,

$$\hat{x}[n] \xrightarrow{\text{m.s.}} \mu_c\, x[n] + v[n], \tag{I.27}$$

where $v[n]$ is a complex-valued, marginally Gaussian, zero-mean white noise sequence, un-

[5]We use the notation $\xrightarrow{\text{m.s.}}$ to denote, specifically, convergence in the mean-square sense.

correlated with the input symbol sequence $x[n]$ and having variance

$$\operatorname{var} v[n] = \mathcal{E}_s\sigma_c^2 + \mathcal{N}_0\mathcal{W}_0(\sigma_b^2 + |\mu_b|^2). \tag{I.28}$$

Effectively, Theorem 1 asserts that the use of sufficient precoding transforms the channel "seen" by the coded symbol stream from a fading channel into a marginally Gaussian white noise channel with no intersymbol interference. As a result, the characteristics of the composite channel depend only on the statistics of the fading channel parameters $a[n;k]$ and $w[n]$ but *not* on the values of the parameters themselves. Not surprisingly, this is a natural consequence of the time averaging induced by precoding being applied to an ergodic fading process.

A few additional remarks regarding Theorem 1 are appropriate. First, as can be readily verified from the proof in Appendix III.A, Theorem 1 is in fact true even when the kernel $a[n;k]$ and receiver noise $w[n]$ are not Gaussian. This observation is important in terms of robustness, since these processes are of course at most approximately Gaussian in practice.

Second, we emphasize that $v[n]$ in Theorem 1 is a marginally Gaussian process. Specifically, this means that $v[n]$ is a sequence of uncorrelated random variables each having a Gaussian distribution, but that the random variables are not necessarily jointly Gaussian. Hence, $v[n]$ is not necessarily a Gaussian random process, and, as a result, there may exist at least some statistical dependence among the noise samples. However, we shall assume that, in practice, $v[n]$ is an at least approximately Gaussian process, so that the statistical dependency among samples is, in some sense, negligible.

The noise $v[n]$ has other special characteristics as well. As is apparent from (I.28), the noise consists of the sum of two uncorrelated components. The first component has power $\mathcal{N}_0\mathcal{W}_0(\sigma_b^2 + |\mu_b|^2)$ and is due to the noise in the original fading channel. The second component has power $\mathcal{E}_s\sigma_c^2$ and is inherently generated in the precoding process. The existence of this second noise component means that boosting the transmitter power in the system also leads to an increase in noise power in the composite channel. For this reason, we shall find that the familiar matched-filter equalizer [14] is not best suited for use with precoding.

Finally, we point out that although Theorem 1 establishes only an asymptotic result valid for perfectly lossless precoding with infinite dispersion (implying, for example, infinite delay), the asymptotic behavior can be approximated arbitrarily closely with realizable precoders. In particular, with suitably chosen finite length precoders, the white marginally Gaussian channel model is an excellent approximation to the actual composite channel. Furthermore, the delay requirements in this case are comparable to those of conventional interleaving. Specifically, the filter length N required to effectively converge to the equivalent model is given by

$$N \approx N'(\tau_a + 1) \tag{I.29}$$

where N' is the length required in the case of memoryless fading, and where τ_a is the

coherence time of the fading channel (in samples). Specifically,

$$\tau_a = \frac{1}{\sigma_a^2} \sum_{m=1}^{\infty} \Psi_a(0;m] = \left(\frac{1}{\sigma_a^2} \sum_{m=0}^{\infty} \Psi_a(0;m] \right) - 1 \tag{I.30}$$

where, defined according to (I.20), $\Psi_a(\omega;m]$ is the original channel's spaced-frequency spaced-time correlation function. We can alternatively express τ_a in terms of the (double-sided) Doppler spread of the fading channel δ_a, which we define as

$$\delta_a = \frac{\int_{-\infty}^{\infty} \Upsilon_a(\lambda)\, d\lambda}{\Upsilon_a(0)} \tag{I.31}$$

where, defined according to (I.23), $\Upsilon_a(\lambda)$ is the Doppler power spectrum of the channel. In particular, comparing (I.31) with (I.30) we see that our definitions of coherence time and Doppler spread are related according to

$$1 + 2\tau_a = 2\pi/\delta_a.$$

Later we discuss appropriate values for N' in practice.

It is important to note that while large coherence times (or, equivalently, small Doppler spreads) correspond to larger inherent delays in the system, they need not incur additional computational complexity either at the transmitter or receiver. In fact, from a single prototype precoder $h[n]$ one can derive an entire family of precoders with the same loss, dispersion, energy, and computational characteristics but suitable for scenarios corresponding to different coherence-time/Doppler-spread parameters. Specifically, if $h[n]$ is a precoder designed for memoryless fading ($\tau_a = 0$), then the corresponding precoder $h_{\tau_a}[n]$ for the case in which the fading has coherence time τ_a is obtained by simply upsampling $h[n]$, *i.e.*,

$$h_{\tau_a}[n] = \begin{cases} h[n/M] & n = \cdots, -M, 0, M, 2M, \cdots \\ 0 & \text{otherwise} \end{cases} \tag{I.32}$$

where[5]

$$M = \lceil \tau_a + 1 \rceil$$

is the upsampling factor. Equivalently, this upsampling relationship can be described in the frequency domain as

$$H_{\tau_a}(\omega) = H(M\omega). \tag{I.33}$$

Using both (I.32) and (I.33) one can verify that the energy, loss, dispersion, and computational characteristics are unaffected by such upsampling.

Let us now consider the design of the equalizer. We begin by observing that Theorem 1 implicitly imposes certain constraints on the equalizer kernel $b[n;k]$ in order that the equivalent channel model structure is attained asymptotically. These constraints are, from a practical standpoint, in fact relatively mild. Specifically, it suffices that $b[n;k]$ be chosen so

[5]The ceiling function $\lceil x \rceil$ denotes the smallest integer greater than or equal to x.

that both $b[n;k]$ and the cascade of $a[n;k]$ with $b[n;k]$, (*i.e.*, (I.26)) are admissibly ergodic. For convenience, let us refer to kernels $b[n;k]$ with this property as *admissible* equalizers.

Among the class of admissible equalizers, some yield better composite channels than others. One useful measure of the quality of the composite channel is the signal-to-noise ratio (SNR). Certainly when $v[n]$ is Gaussian the both the theoretical capacity and achievable bit error rates increase monotonically with the channel SNR. Consequently, a useful criterion for equalizer design is to select among the admissible equalizers that yielding the largest SNR in the composite channel. Conveniently, when $b[n;k]$ is an admissible equalizer, the SNR in the composite channel follows directly from Theorem 1 as

$$\gamma(b) = \frac{|\mu_c|^2}{\sigma_c^2 + \xi_0 \left(\sigma_b^2 + |\mu_b|^2\right)} \tag{I.34}$$

where

$$\xi_0 = \mathcal{N}_0 \mathcal{W}_0 / \mathcal{E}_s. \tag{I.35}$$

In Sections I.4.1 and I.4.2, we proceed to derive these optimum equalizers in the two cases of perhaps greatest interest in practice, corresponding to frequency-nonselective fading and frequency-selective slow fading, respectively.

I.4.1 Frequency-Nonselective Fading

In this section, we restrict our attention to the Rayleigh fading channel model of (I.1) with

$$a[n;k] = a[n]\,\delta[k].$$

in which case, as is straightforward to show, the admissible equalizers are also of the form

$$b[n;k] = b[n]\,\delta[k].$$

Accordingly, we may rewrite (I.34) in this scenario as

$$\gamma(b) = \frac{|E\,[ab]|^2}{\mathrm{var}\,[ab] + \xi_0 E\,[|b|^2]}, \tag{I.36}$$

where ξ_0 is as defined in (I.35) and where we have omitted a specification of the time sample n due to stationarity.

To derive the optimum equalizer, we begin by rewriting (I.36) as

$$\gamma(b) = \frac{1}{1/\varphi(b) - 1} \tag{I.37}$$

where

$$\varphi(b) = \frac{|E\,[ab]|^2}{E\,[(|a|^2 + \xi_0)|b|^2]}, \tag{I.38}$$

and where we have exploited the identity

$$\mathrm{var}\,[ab] = E\left[|ab|^2\right] - |E\,[ab]|^2.$$

Then, by the Schwarz inequality we have

$$|E[ab]|^2 = \left| E\left[\frac{a}{\sqrt{|a|^2+\xi_0}} \cdot b\sqrt{|a|^2+\xi_0} \right] \right|^2 \leq E\left[\frac{|a|^2}{|a|^2+\xi_0} \right] E\left[(|a|^2+\xi_0)|b|^2 \right]$$

with equality if and only if

$$b \propto \frac{a^*}{|a|^2+\xi_0}.$$

Hence, (I.38), and, in turn, (I.36) are maximized when

$$b[n] \propto \frac{a^*[n]}{|a[n]|^2+\xi_0}, \tag{I.39}$$

where the (complex) constant of proportionality is arbitrary.

Not surprisingly, the optimum equalizer is specified only to within an arbitrary gain factor, since such factors do not affect the resulting SNR. In addition, it is interesting to note (and can be readily verified) that the equalizer yielding optimum SNR in the composite channel, *i.e.*, (I.39), also corresponds, when suitably normalized, to a minimum mean-square error linear equalizer for the fading channel. Specifically, $\hat{y}[n]$ and, in turn, $\hat{x}[n]$ are minimum mean-square error linear estimates of $y[n]$ and $x[n]$, respectively. Although he did not establish its optimality, it was Wittneben [4] in his preliminary work on precoding for the nonselective fading channel with interleaving who first suggested that a minimum mean-square error type equalizer was well-suited to this scenario.

I.4.2 Frequency-Selective Fading

In this section, we consider the more general channel model (I.1) for which the fading is, in general, frequency selective. This scenario generally arises when larger transmission bandwidths are used, as is often desirable to achieve additional diversity benefit. Furthermore, in deriving the corresponding optimum equalizers, we exploit the fact that in this case the fading process becomes increasingly slowly-varying as the bandwidth is expanded.

Accordingly, we begin by assuming that the coherence time in the channel is large, so that the fading coefficients are effectively constant over a several time samples. Then the time-variant channel frequency response $A(\omega;n]$ will vary slowly with n, and admissible equalizers will also have a slowly-varying time-variant frequency response $B(\omega;n]$. Furthermore, we have

$$C(\omega;n] \approx A(\omega;n]\,B(\omega;n]. \tag{I.40}$$

Now (I.19) and (I.25) imply

$$\mu_c = E[C(\omega;n]] \tag{I.41a}$$

$$\sigma_c^2 = \mathrm{var}[C(\omega;n]] \tag{I.41b}$$

and

$$\sigma_b^2 + |\mu_b|^2 = E\left[|B(\omega;n]|^2\right]. \tag{I.41c}$$

Hence, using (I.41) with (I.40) in (I.34), we get that the channel SNR is effectively given

by

$$\gamma(b) \approx \frac{|E[AB]|^2}{\mathrm{var}[AB] + \xi_0 E[|B|^2]}, \tag{I.42}$$

where, again, ξ_0 is as given by (I.35), and where we have omitted specification of both the time sample n and frequency value ω due to stationarity. Clearly, (I.42) is identical in form to (I.36), and, consequently, the equalizer providing the best SNR for the composite channel follows analogously as

$$B(\omega; n] \propto \frac{A^*(\omega; n]}{|A(\omega; n]|^2 + \xi_0} \tag{I.43}$$

where, again, the (complex) constant of proportionality is arbitrary. As in the nonselective fading case, we remark that this equalizer not only maximizes the channel SNR but also, when suitably normalized, makes $\hat{x}[n]$ a minimum mean-square error linear estimate of $x[n]$.

The receiver structure in this frequency-selective scenario warrants some additional discussion. With $b[n; k]$ varying slowly with n, let us denote by $b[k]$ the nominal value of $b[n; k]$ over some sufficiently long generic time interval. To implement the unit-sample response $b[k]$, it is useful, at least conceptually, to view the equalization process in two stages. The first stage implements the numerator of (I.43), and corresponds to the appropriate matched-filter equalizer, and, hence, is a conventional RAKE receiver [1]. The unit-sample response of this stage is, therefore, $a^*[-k]$. The second stage, which implements the denominator of (I.43), then performs additional compensation, taking into account the SNR in the channel. The unit-sample response corresponding to this second stage, which we denote by $e[k]$, is symmetric and, in general, infinite in extent (hence, two-sided), precluding any recursive implementation. However, typically, the tails of the unit-sample response fall off quickly. In particular, when $a[k]$ is non-zero for only finitely many values of k as is frequently assumed in practice, $e[k]$ decays exponentially quickly with k. Hence, using truncation $e[k]$ may be effectively approximated as a symmetric FIR filter. As an example, Fig. I.2 depicts the normalized RMS value of the coefficient $e[k]$, *viz.*,

$$\sqrt{E[|e[k]|^2] / E[|e[0]|^2]},$$

as a function of k, where

$$E\left[|a[k]|^2\right] = \begin{cases} 1/2 & k = 0, 1 \\ 0 & \text{otherwise} \end{cases}. \tag{I.44}$$

and where $\xi_0 = \sigma_a^2$.

I.5 Performance

In this section, we explore the potential performance achievable through the use of spread-response precoding with optimized receivers. We begin by observing that with the optimum equalizer, *i.e.*, (I.39) in the case of frequency nonselective fading or (I.43) in the case of frequency selective fading, we readily obtain that the corresponding SNR in the composite

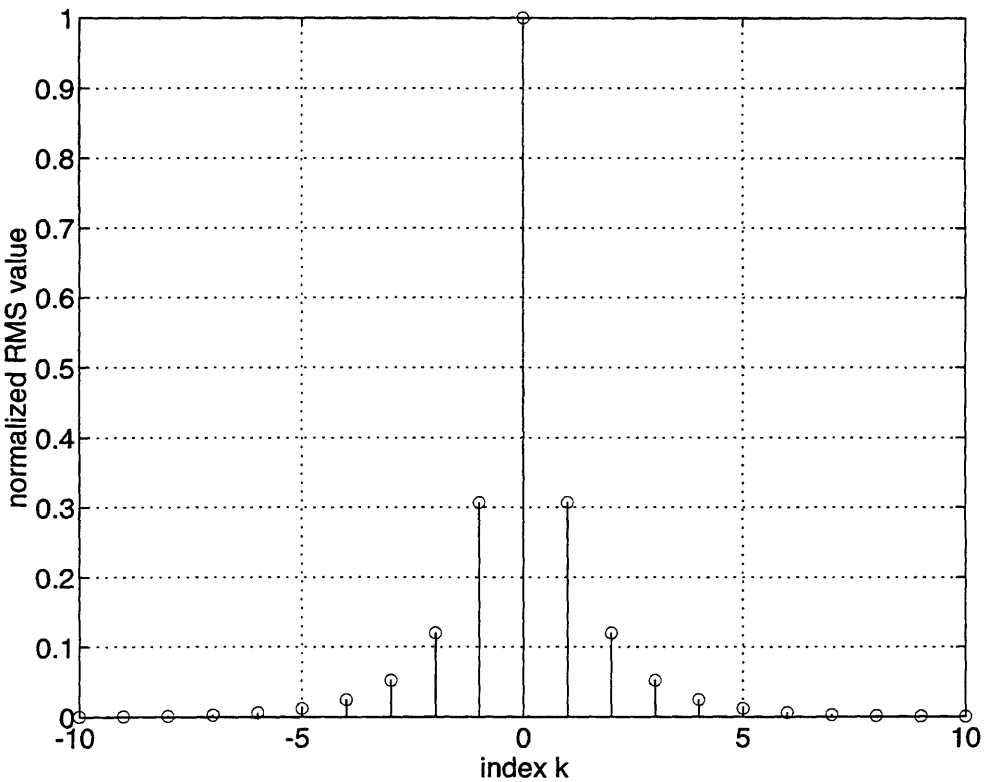

Figure I.2: *A typical RMS unit-sample response of the second stage of equalizer. In this example, the variances of the fading coefficients $a[k]$ were chosen according to (I.44), and the SNR was chosen so that $\xi_0 = \sigma_a^2$.*

channel is given by

$$\gamma_0 = \frac{1}{E\left[\frac{1}{\gamma_0+1}\right]} - 1 \tag{I.45}$$

where[6]

$$\gamma_0 = \frac{|A(\omega;n)|^2\mathcal{E}_s}{\mathcal{N}_0\mathcal{W}_0} \tag{I.46}$$

denotes the SNR in the original fading channel at a particular time instant n and frequency ω. A useful notion of the capacity of the composite channel is given by the equivalent Gaussian capacity[7], *i.e.*, using (I.45),

$$\mathcal{C}/\mathcal{W}_0 = -\log(1+\gamma_0) = -\log\left(E\left[\frac{1}{\gamma_0+1}\right]\right). \tag{I.47}$$

Exploiting the readily verified identity

$$E\left[\log(\gamma_0+1)\right] = \frac{1}{\zeta_0}E\left[\frac{1}{\gamma_0+1}\right] = e^{\zeta_0}E_1(\zeta_0) \tag{I.48}$$

where

$$1/\zeta_0 \triangleq E\left[\gamma_0\right] = \frac{\sigma_a^2\mathcal{E}_s}{\mathcal{N}_0\mathcal{W}_0} \tag{I.49}$$

denotes the average SNR in the original fading channel (*cf.* (I.4b)), and $E_1(\cdot)$ denotes the exponential integral [15]

$$E_1(\nu) = \int_\nu^\infty \frac{e^{-t}}{t}\,dt, \tag{I.50}$$

we get that (I.51) can be expressed more conveniently as

$$\mathcal{C}/\mathcal{W}_0 = -\log\left(\zeta_0 e^{\zeta_0}E_1(\zeta_0)\right). \tag{I.51}$$

The capacity estimate (I.51) can be compared to some related capacity calculations. In particular, by the Schwarz inequality we get

$$E\left[\frac{1}{\gamma_0+1}\right] \geq \frac{1}{E\left[\gamma_0+1\right]} = \frac{1}{1+1/\zeta_0},$$

so that, as expected, (I.51) is upper bounded by the capacity of the Gaussian channel or, equivalently, the fading channel with infinite spatial diversity, *i.e.*,

$$\mathcal{C}_\infty/\mathcal{W}_0 = \log\left(1+E\left[\gamma_0\right]\right) = \log\left(1+1/\zeta_0\right). \tag{I.52}$$

More generally, there have been a variety of attempts to estimate the capacity of fading channels in the literature [5]. As an example, between $\mathcal{C}$ and $\mathcal{C}_\infty$ lies the estimate of fading

[6]Of course, in the case of nonselective fading $A(\omega;n] = a[n;0] = a[n]$ using the notation of Section I.4.1.

[7]More precisely, this can be interpreted as a constrained capacity—specifically the bit rate that can be achieved when the remaining higher-order statistical dependencies in the composite channel model are not exploited.

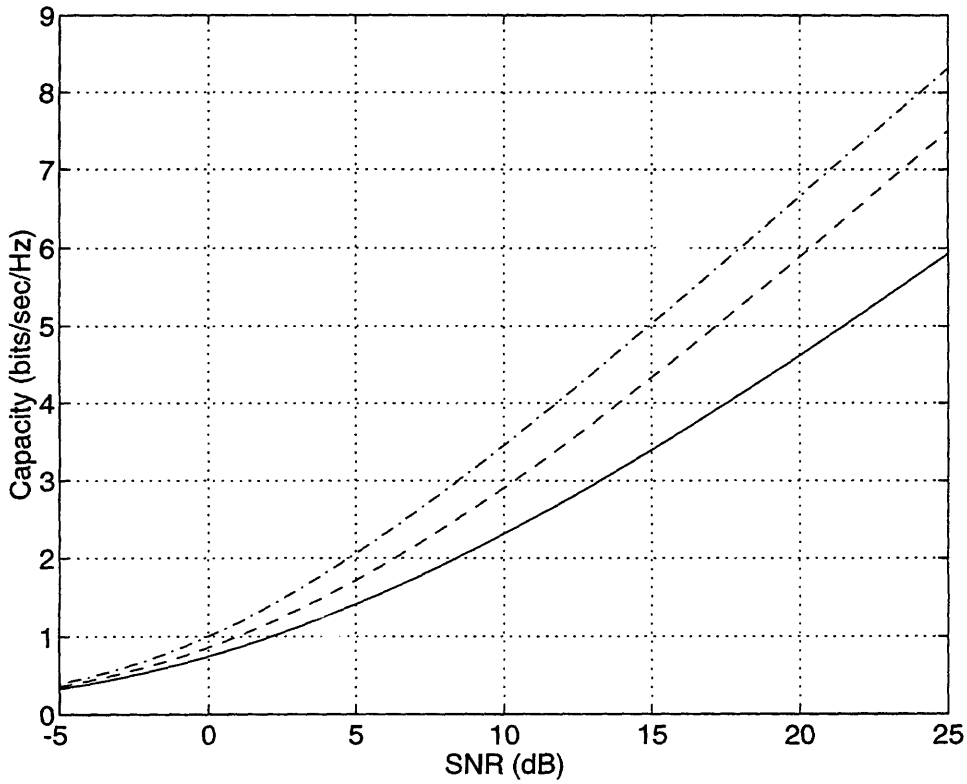

Figure I.3: *Capacity estimates, Rayleigh fading channel. The solid curve is the capacity estimate C determined using precoding. For comparison, the dotted curve is the capacity C_∞ when infinite spatial diversity is available, while the dashed curve is the capacity estimate C_0 due to Lee [16].*

channel capacity without spatial diversity derived by Lee [16], *i.e.*,

$$C_0/\mathcal{W}_0 = E\left[\log\left(1+\gamma_0\right)\right] = e^{\zeta_0}\, E_1(\zeta_0), \tag{I.53}$$

where the second equality follows from (I.48). In Fig. I.3, these capacity estimates (in bits/sec/Hz) are plotted as a function of the average available SNR. The capacities C, C_0, and C_∞ are represented by the solid, dashed, and dotted curves, respectively.

At high SNR (*i.e.*, small ζ_0), we can use the series expansion [15]

$$E_1(\nu) = -\Gamma_0 - \log\nu - \sum_{k=1}^{\infty} \frac{(-1)^k\,\nu^k}{k\,k!}, \tag{I.54}$$

where $\Gamma_0 = 0.57721\cdots$ is Euler's constant, to show that (I.51) is given asymptotically by

$$\mathcal{C}/\mathcal{W}_0 \sim \log\left(\frac{1/\zeta_0}{\log(1/\zeta_0)}\right). \tag{I.55}$$

By contrast, in the same regime (I.52) behaves like

$$\mathcal{C}_\infty/\mathcal{W}_0 \sim \log(1/\zeta_0) \tag{I.56}$$

while (I.53), as can be shown via (I.54), satisfies

$$\mathcal{C}_0/\mathcal{W}_0 \sim \Gamma_0 + \log(1/\zeta_0). \tag{I.57}$$

Hence, comparing (I.57) with (I.56) and (I.55) we can verify that at high SNR the difference between $\mathcal{C}_\infty$ and $\mathcal{C}_0$ is approximately 2.506 dB while the difference between $\mathcal{C}_0$ and $\mathcal{C}$ diverges to infinity.

We stress that these capacity estimates correspond to the case in which the transmitter has no knowledge of the state of the fading channel or its statistics at any point in time, *i.e.*, there is no side-channel for feedback from the receiver to the transmitter. We note, however, because of memory in the fading channel, the availability of a feedback path would naturally lead to higher capacity [17].

We also remark that to approach the capacity $\mathcal{C}$ of the composite channel requires, of course, that coding be applied to the data stream prior to precoding. However, because the composite channel is effectively an additive white Gaussian noise channel, any of the traditional forms of coding for this channel would be appropriate. In particular, we note that conventional implementations of trellis-coded modulation appear to be well-suited to this scenario.

Nevertheless, even without coding significant improvements in bit error rate performance can be achieved from the inherent diversity benefit of using spread-response precoding. We emphasize that this is in marked contrast to the use of interleaving, which offers no improvement in bit error rate performance without coding. For the purposes of illustration, let us consider the case in which $x[n]$ is an uncoded QPSK (quadrature phase-shift keying) stream. When precoding is used, the bit error probability as a function of the SNR per bit, *i.e.*,

$$\frac{\mathcal{E}_b\sigma_a^2}{\mathcal{N}_0\mathcal{W}_0} = \frac{\mathcal{E}_s\sigma_a^2}{2\mathcal{N}_0\mathcal{W}_0},$$

is given by

$$\mathcal{P} = \mathcal{Q}\left(\sqrt{\gamma}\right) \tag{I.58}$$

where

$$\mathcal{Q}(\nu) = \frac{1}{\sqrt{2\pi}}\int_\nu^\infty e^{-t^2/2}\,dt,$$

and where γ, via (I.45) with (I.46), is given by

$$\gamma_0 = \frac{1}{\zeta_0\, e^{\zeta_0}\, E_1(\zeta_0)} - 1$$

with ζ_0 given by (I.49). For comparison, without precoding the QPSK bit error probability using L-fold spatial diversity and maximal ratio combining is given by [1]

$$\mathcal{P}_0[L] = \frac{1}{2}\left[1 - \frac{1}{\sqrt{2\zeta_0 L + 1}} \sum_{k=0}^{L-1} \binom{2k}{k} \left(\frac{\zeta_0 L}{2(2\zeta_0 L + 1)}\right)^k\right]. \tag{I.59}$$

Furthermore, (I.59) specializes to

$$\mathcal{P}_0[1] = \frac{1}{2}\left(1 - \frac{1}{\sqrt{2\zeta_0 + 1}}\right)$$

when there is no spatial diversity, and to

$$\mathcal{P}_0[\infty] = \mathcal{Q}\left(\sqrt{E[\gamma_0]}\right) = \mathcal{Q}\left(1/\sqrt{\zeta_0}\right) \tag{I.60}$$

when there is infinite spatial diversity. In Fig. I.4, we plot bit error probability as a function of SNR per bit (*i.e.*, $1/(2\zeta_0)$) with and without precoding. The solid curve in Fig. I.4 corresponds to the use of precoding (with infinite dispersion) but no spatial diversity. The dashed curves correspond to the use of no precoding but L-fold diversity for $L = 1, 2, \ldots, 5$. Finally, the dotted curve corresponds to the use of no precoding but infinite spatial diversity, $L \to \infty$.

Comparing $\mathcal{P}$ with $\mathcal{P}_0[1]$ we see that precoding markedly improves bit error rate performance in the channel. We can further show, by applying (I.54) and the asymptotic expansion [15]

$$\mathcal{Q}(\nu) \sim \frac{1}{\sqrt{2\pi}\nu} e^{-\nu^2/2} \sum_{k=0}^{\infty} \frac{(-1)^m (2m)!}{2^m m!} \nu^{-2m} \tag{I.61}$$

to (I.58), that at high SNR (*i.e.*, small ζ_0) the bit error rate with precoding is given by

$$\mathcal{P} \sim \sqrt{\frac{\log(1/\zeta_0)}{1/\zeta_0}} \exp\left(-\frac{1/(2\zeta_0)}{\log(1/\zeta_0)}\right) \tag{I.62}$$

By contrast, in the high SNR regime, $\mathcal{P}_0[L]$ is well-approximated as [1]

$$\mathcal{P}_0[L] \sim \zeta_0^L,$$

while (I.60), via (I.61), takes the form

$$\mathcal{P}_0[\infty] \sim \sqrt{\zeta_0} e^{-1/(2\zeta_0)}.$$

Thus, we note that the while $\mathcal{P}$ falls off at a slower rate than $\mathcal{P}_0[\infty]$, it falls off faster than $\mathcal{P}_0[L]$ for any fixed L. This implies that, asymptotically, precoding provides higher "effective diversity" than can be achieved using spatial diversity with any $L < \infty$, but less than can be achieved with infinite spatial diversity.

While the solid curve in Fig. I.4 is obviously a lower bound on the bit error rate performance achievable in practice using finite length precoders, it is quite realistic when the precoding filter has length N given by (I.29) for $N' \sim 100$. In Fig. I.5, we plot bit error

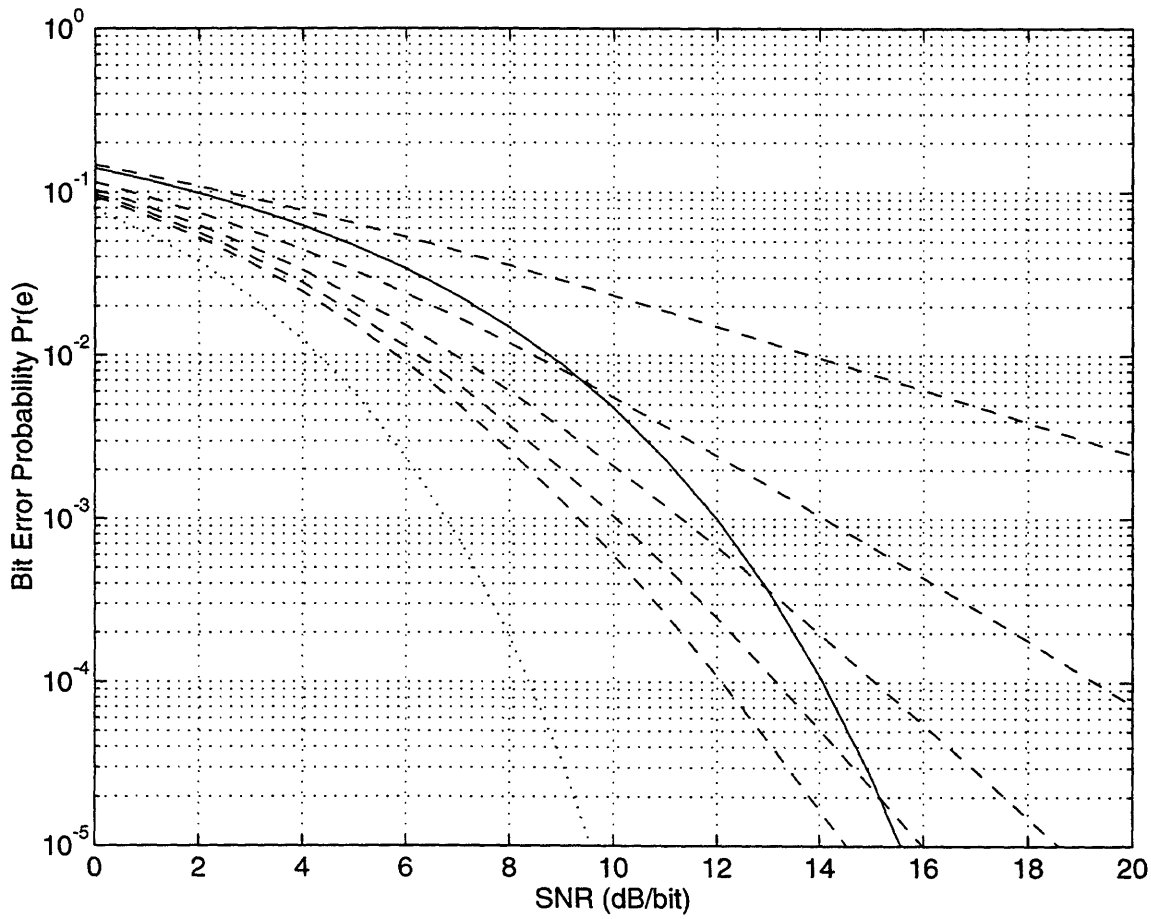

Figure I.4: *Bit error probabilities using uncoded QPSK on the Rayleigh fading channel. The solid curve represents the performance achievable with precoding. For comparison, also depicted is the attainable performance without precoding but, instead, with spatial diversity and maximal ratio combining. The dotted curve corresponds to the performance with infinite spatial diversity, while the successively lower dashed curves correspond to the performance with* $L = 1, 2, \ldots, 5$ *branches of spatial diversity, respectively.*

probability for uncoded QPSK as a function of SNR per bit using realizable precoders. The solid curve indicates the infinite dispersion bound, while the successively lower broken curves indicate the performance with practical precoders corresponding to $N' = 27$ and $N' = 200$, respectively.

Finally, we remark that experiments exploring the sensitivity of system performance to the parameters of the equalizer, while beyond the scope of this report, are clearly warranted in the future. In the meantime, preliminary simulations reported in [4] involving minimum mean-square error type equalizers lend at least some insight into what kind of behavior may be expected. Specifically, the results suggest that performance ought to depend only weakly on the estimate of $\mathcal{E}_s/(\mathcal{N}_0\omega_0)$ used in the equalizer, and that the performance can be expected to degrade fairly gracefully with errors in estimates of the magnitude and phase of the fading coefficients.

I.6 Summary

Spread-response precoding as developed in this part of the report constitutes a potentially attractive alternative to interleaving in a wide range of communication systems designed for use with multipath fading channels. Even when no additional coding is used, precoding can significantly improve system performance over other uncoded systems. Similarly, the use of precoding in conjunction with coding has the potential to substantially reduce computational complexity at both the transmitter and the receiver for a given level of performance. This is because the effects of fading are entirely controlled by the precoding, which requires only low-complexity signal processing. Thus, only additive noise remains for coding to control, which can in turn be achieved with comparatively shorter codes. As an additional potential feature, the noise-like characteristics of the transmitted stream resulting from the use of precoding appears to be well-suited for applications involving secure communication.

Nevertheless, several technical issues remain to be explored. For example, a detailed investigation of the complexity benefits that can be realized through the use of precoding with coding is clearly warranted. The development of techniques for adequately synchronizing the receiver in such systems as well as for managing the inherent peak-to-average power requirements is also an important avenue for future research. Furthermore, in order for precoding to be effective, reliable estimates of the fading channel parameters and statistics must be available at the receiver. It appears that this can be accomplished in practice through the use of training sequences or decision feedback techniques. However, such issues remain to be explored in detail. Finally, as remarked earlier, regardless of the technique used, any such parameter estimates are imperfect and, as a result, sensitivity analysis would ultimately be important in further verifying the viability of spread-response precoding.

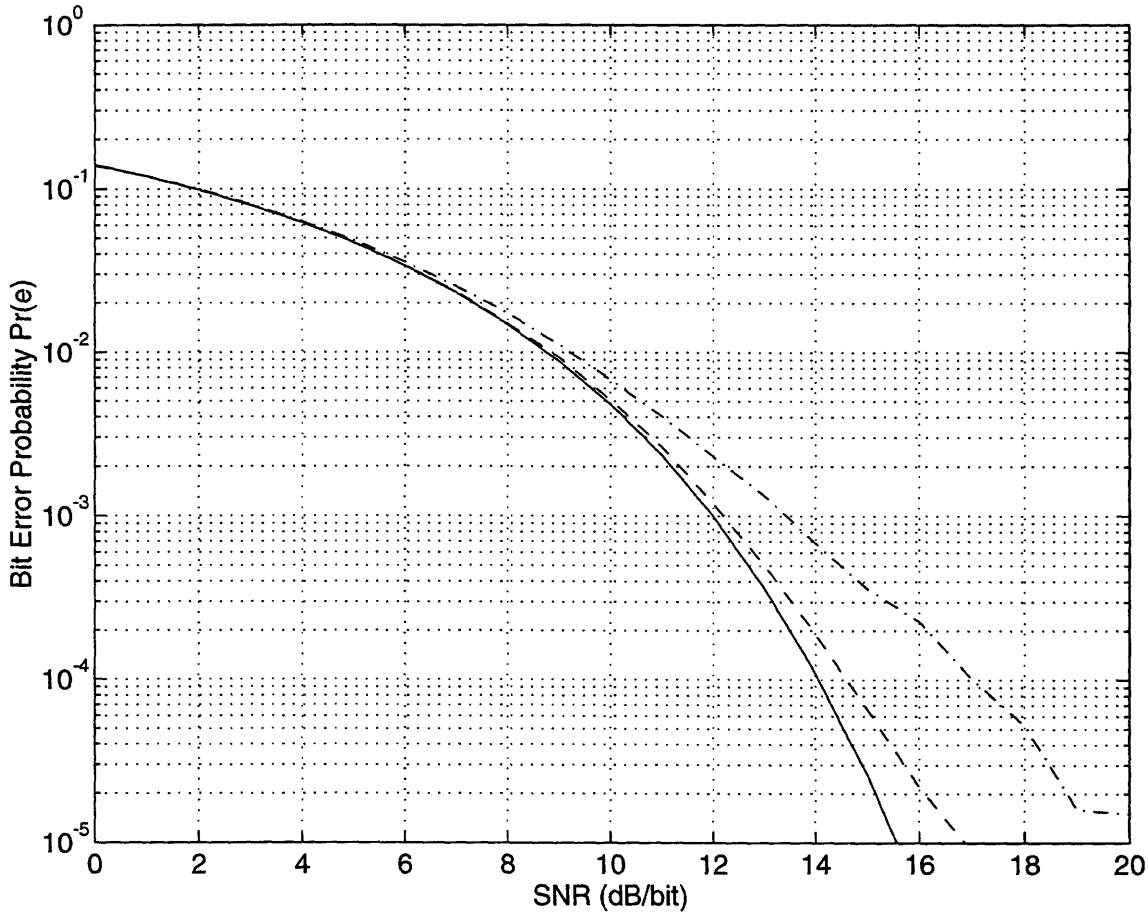

Figure I.5: *Bit error probabilities using uncoded QPSK on the Rayleigh fading channel with realizable precoders. The dash-dotted and dashed curves represent the performance obtained using FIR precoders with* $N' = 27$ *and* $N' = 200$*, respectively. The solid curve represents the ideal precoder performance bound* ($N' \to \infty$).

Part II

Spread-Signature Code-Division Multiple Access

II.1 Introduction

Systems for efficiently coordinating communication among multiple users in multipath fading environments are important in a wide range of applications. Indeed, such systems are essential in proposed digital mobile radio communications, personal wireless systems, indoor wireless networks, and digital audio and television broadcasting systems. However, rapidly escalating demand for both wider availability of such services and increasingly sophisticated capabilities has put great pressure on the limited available bandwidth within the radio spectrum. Given such constraints, it is clear that the use of increasingly sophisticated signal processing in wireless modems will be critical to accommodating large numbers of services and users within the available spectrum.

In Part I, we explored the use of spread-response precoding for mitigating the effects of fading in single-user or frequency-division multiplexed data transmission systems used in multipath fading environments. From the perspective of the coded symbol stream, this precoding effectively transforms a fairly general Rayleigh fading channel into a nonfading, simple white marginally Gaussian additive noise channel with no intersymbol interference. By using such precoding to combat fading while reserving coding to combat only the remaining additive noise, substantial reductions in system complexity appear possible. Furthermore, although spread-response precoding represents a form of time-diversity, it is efficient in the sense that it requires no additional power or bandwidth.

In this part of the report, we develop a natural generalization of the precoding concept for general multiuser communication problems in multipath fading environments. The result is a code-division multiple-access (CDMA) system in which, in effect, precoding is embedded directly into each user's signature sequence while maintaining orthogonality among users. We term the resulting system "spread-signature CDMA." These signature sequences have some very special characteristics as we will show, most notable of which is that their temporal extent significantly exceeds the intersymbol (baud) duration.

In a manner analogous to spread-response precoding, using such signature sets in multipath fading environments has the effect of transforming the collection of channels seen by

the individual symbol streams from a collection of coupled Rayleigh fading channels into a uncorrelated collection of identical nonfading simple white marginally-Gaussian additive noise channels. In essence, spread-signature CDMA converts various degradations due to fading, co-channel interference, and receiver noise into a single, comparatively more benign form of uncorrelated additive noise that is white and quasi-Gaussian.

Transformations of this type are, in general, highly desirable in multiuser systems; see, *e.g.*, [18]. As we will see, spread-signature CDMA systems provides some important potential performance advantages over traditional CDMA systems. Furthermore, we will see that spread-signature CDMA systems achieve this benefit without requiring additional power or bandwidth, and are attractive in terms of computational complexity, robustness, and delay considerations.

Our model consists of a fairly general cellular multiple-access scenario in which each cell contains a single base station (sometimes referred to as a "cell site") and a number of mobiles (or, more generally, "subscribers"). We assume that both forward link (base-to-mobile) and reverse link (mobile-to-base) communication is required, but takes place on separate (*i.e.*, non-interfering) channels. Between each transmitter-receiver pair is a fairly general Rayleigh fading channel, which may be frequency selective or non-selective.

The outline of the Part II is as follows. In Section II.2, we develop the equivalent discrete-time baseband model for our multiuser system and some basic notation. In Section II.3, we then develop a useful framework for characterizing the generalized orthogonal CDMA signature sets of interest in this work, and use this framework to develop an efficient family of spread-signature sets. Section II.4 develops some important aspects of spread-signature CDMA systems, ranging from transmission characteristics to channel-transformation properties of such systems. We then exploit these properties to develop efficient spread-signature CDMA receivers. Section II.5 explores the potential performance of such optimized systems both in terms of capacity and bit error rate characteristics, and Section II.6 contains some concluding remarks.

II.2 System Model

Consider a single cell of a multiple-access system, in which there are M users, all sharing a total fixed bandwidth MW_0, so that W_0 is the effective bandwidth per user. In the equivalent discrete-time baseband model for the system, the modulation process can be viewed as follows. The coded symbol stream of the mth user ($1 \leq m \leq M$), which we denote by $x_m[n]$, is modulated onto a unique signature sequence $h_m[n]$ to produce $y_m[n]$ which is transmitted within the total available bandwidth.

Conceptually, it is convenient to view the modulation process in two stages. As depicted in Fig. II.1, these stages correspond to upsampling (*i.e.*, zero-insertion) by a factor M, followed by linear time-invariant filtering with the signature sequence, *i.e.*,

$$y_m[n] = \sum_k x_m[k]\, h_m[n - kM]. \tag{II.1}$$

The multiuser channel we consider, which is depicted in Fig. II.2, is a rather general stationary Raleigh fading environment with uncorrelated scattering. More specifically, $a_m[n; k]$

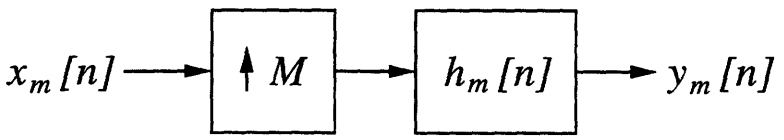

Figure II.1: *Modulation of the the mth user's coded symbol stream $x_m[n]$ onto a signature sequence $h_m[n]$ for transmission.*

represents the zero-mean, complex-valued Gaussian kernel of the fading channel seen by that user. Hence, the sequence obtained at the receiver is

$$r[n] = \sum_m \sum_k a_m[n;k]\, y_m[n-k] + w[n] \tag{II.2}$$

where $w[n]$ is a zero-mean, complex-valued stationary white Gaussian sequence with variance[1]

$$E\left[|w[n]|^2\right] = \mathcal{N}_0 \mathcal{W}_0 \tag{II.3}$$

that is statistically independent of both the $a_m[n;k]$ and the $y_m[n]$. In general, the randomly time-varying kernels $a_m[n;k]$ capture the effects of multipath fading due to both fluctuations in the media and the relative motions of transmitters and receivers in the system. Meanwhile, $w[n]$ captures both receiver noise and any sources of co-channel interference not otherwise taken into account. We use $A_m(\omega;n]$ to denote the (stationary) time-variant frequency response corresponding to the mth channel. Our notation for characterizing other aspects of this class of linear randomly time-varying systems, which is essentially the same as was used in Part I, is summarized for convenience in Appendix III.B.

Two special cases of this general channel model are of primary interest. The first, corresponding to base-to-mobile transmission, is referred to as the forward link. In this case, the messages to the individual mobiles are multiplexed together before being broadcast over the channel. From the perspective of a particular receiver all messages are transmitted through the same channel, *i.e.*,

$$a_1[n;k] = a_2[n;k] = \cdots = a_M[n;k] \triangleq a[n;k]. \tag{II.4}$$

The second case, corresponding to mobile-to-base transmission, is referred to as the reverse link. In this case, the messages are transmitted through separate channels to the base station. With reasonable physical separation among mobiles, as we will assume, the kernels of the individual mobile-to-base channels may be modeled as mutually independent. We shall further assume that no base-to-mobile feedback channel is available to provide synchronization information to the mobiles. Accordingly, the kernels $a_m[n;k]$ in our model capture the effects of both multipath fading and asynchronism among users.

[1]Note that, for convenience, in our equivalent model the channel parameters are bandwidth-normalized, *i.e.*, the statistics of both $a_m[n;k]$ and $w[n]$ are independent of the bandwidth parameter M. To maintain the proper dependence of signal-to-noise ratio on M, we therefore bandwidth-normalize the transmitted power as well. Indeed, as we will establish in Section II.4.1, when the coded stream $x_m[n]$ has power $\mathcal{E}_m$, the transmitted stream $y_m[n]$ has power $\mathcal{E}_m/M$.

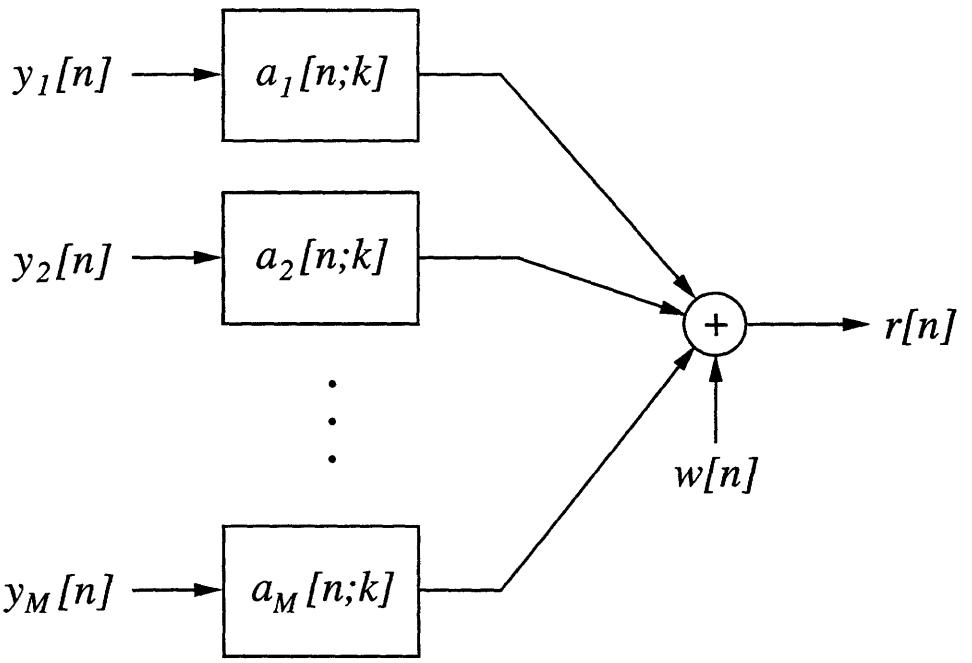

Figure II.2: *General multiuser fading channel model, where $a_m[n;k]$ denotes the randomly time-varying linear kernel corresponding to the mth user.*

Finally, we make the reasonable assumption that, in both forward and reverse link cases, while the transmitters have no knowledge of the channel kernels $a_m[n;k]$ or their statistics, these parameters are known—or, more typically, can be reliably measured—at the corresponding receivers in the system.

II.3 Orthogonal Multiuser Modulation

In traditional CDMA systems, the signature sequences $h_m[n]$ used in the modulation (II.1) have length equal to the upsampling rate or intersymbol period M. In this way the signatures are used in a nonoverlapping manner. However, in this section we consider signatures of arbitrary length N. When $N > M$, the resulting sequences have valuable partial response characteristics akin to those of spread-response precoding, and we refer to these sequences as "spread-signature" sequences.

A useful mathematical framework for representing such signature sets arises out of multirate system theory [19], as we now show. To begin, we first express the signature set as the vector sequence, *i.e.*,[2]

$$\mathbf{h}[n] = \begin{bmatrix} h_1[n] & h_2[n] & \cdots & h_M[n] \end{bmatrix}^T, \tag{II.5}$$

and, for convenience, let us restrict our attention to real-valued signature sets. When each

[2]The superscript ^{T} denotes transposition.

of the component signatures $h_m[n]$ has only finitely many non-zero values, we shall refer to the signature set as having *finite-spread.* Specifically, when

$$\mathbf{h}[n] = \mathbf{0}, \qquad n < 0,\ n \geq N$$

we say that the signature set has *temporal spread* N.

Although the theory can accommodate more general classes of signature sets, we restrict our attention to those satisfying certain convenient orthogonality conditions, which facilitate both analysis and implementation. Specifically, we require that the signature sequences together with all translates by integer multiple of M constitute an orthonormal set, *i.e.*,[3]

$$\sum_k \mathbf{h}[k - nM]\,\mathbf{h}^T[k - mM] = \delta[n - m]\,\mathbf{I} \tag{II.6}$$

where $\mathbf{I}$ denotes the identity matrix of appropriate size, and where $\delta[n]$ denotes the unit sample, *viz.*,

$$\delta[n] \triangleq \begin{cases} 1 & n = 0 \\ 0 & \text{otherwise} \end{cases}. \tag{II.7}$$

In turn, the corresponding completeness condition for this orthonormal set can be expressed as

$$\sum_k \mathbf{h}^T[n - kM]\,\mathbf{h}[m - kM] = \sum_{k,i} h_i[n - kM]\,h_i[m - kM] = \delta[n - m], \tag{II.8}$$

and, in fact, (II.8) can be interpreted as a special instance of Mercer's Theorem [20].

It is important to emphasize that orthonormal signature sets,*i.e.*, sets satisfying (II.6) and (II.8), correspond to lossless systems. As a result, demodulation in the absense of distortion is particularly simple. To illustrate, if the input symbol streams are $x_m[n]$ and the superimposed output is the sequence $y[n]$, *i.e.*, via (II.1),

$$y[n] = \sum_m y_m[n] = \sum_{m,k} h_m[n - Mk]\,x_m[k], \tag{II.9}$$

then the sequences $x_m[n]$ can be reconstructed from $y[n]$ via

$$x_m[n] = \sum_k h_m[k - nM]\,y[k]. \tag{II.10}$$

As we shall see, the discrete-time matched-filter and downsample operation (II.10) is also a key component of the demodulation process when distortion is present as well.

For $M \geq 2$, there is a rich collection of signature sets satisfying (II.6) and (II.8), even when we restrict our attention to signatures with finite-spread. For $M = 1$, however, the modulation process (II.1) is equivalent to prefiltering with a linear time-invariant filter whose unit-sample response is the signature sequence $h_1[n]$. In this case, which was extensively developed in Part I, the condition (II.6) is equivalent to requiring that $h_1[n]$ be an allpass filter, and it is well-known that non-trivial finite-length allpass filters do not exist.

[3]Note that (II.6) directly incorporates the natural requirement that each signature sequence $h_m[n]$ have unit energy.

Several aspects of orthogonal signature sets are more conveniently viewed in the frequency domain. Accordingly, we express the set of Fourier transforms corresponding to (II.5) in the form

$$\mathbf{H}(\omega) = \int_{-\infty}^{\infty} \mathrm{h}[n]\, e^{-j\omega n}\, d\omega \triangleq \left[\begin{array}{cccc} H_1(\omega) & H_2(\omega) & \cdots & H_M(\omega) \end{array} \right]^T. \tag{II.11}$$

For example, the orthogonality properties (II.6) and (II.8) are frequently more conveniently viewed in the frequency domain—as an illustration, (II.8) is equivalent to[4]

$$\mathbf{H}^\dagger(\omega)\, \mathbf{H}(\omega) = \sum_k |H_k(\omega)|^2 = M, \tag{II.12}$$

which is sometimes referred to as a (power) complementarity condition.

More importantly, the frequency domain representation (II.11) leads to the efficient factorization

$$\mathbf{H}(\omega) = \mathbf{Q}(M\omega)\, \mathbf{\Delta}(\omega), \tag{II.13}$$

where $\mathbf{Q}(\omega)$ is a square matrix and $\mathbf{\Delta}(\omega)$ is the Fourier transform of the delay chain of order M, *i.e.*,

$$\delta[n] = \left[\begin{array}{cccc} \delta[n] & \delta[n-1] & \cdots & \delta[n-M+1] \end{array} \right]^T, \tag{II.14}$$

whence

$$\mathbf{\Delta}(\omega) = \left[\begin{array}{cccc} 1 & e^{-j\omega} & \cdots & e^{-j\omega(M-1)} \end{array} \right]^T. \tag{II.15}$$

The decomposition (II.13) is referred to as the *polyphase* representation of the set, and $\mathbf{Q}(\omega)$ is termed the associated polyphase matrix. As is true for multirate systems in general [19], polyphase representations of signature sequences are not only conceptually useful, but lead to computationally efficient modem implementations as well.

For specifically orthonormal signature sets, the associated polyphase matrix satisfies the special property

$$\mathbf{Q}(\omega)\, \mathbf{Q}^\dagger(\omega) = \mathbf{I}, \tag{II.16}$$

and we remark that matrices satisfying (II.16) are termed *paraunitary*. Furthermore, it is straightforward to verify that $\mathbf{Q}(\omega)$ is independent of ω if and only if the signature set is *not* spread (*i.e.*, $N = M$).

The polyphase matrices associated with some familiar orthogonal signature sets provide useful insight. For example, the polyphase matrix corresponding to time-division multiple-access (TDMA) systems is

$$\mathbf{Q}(\omega) = \mathbf{I},$$

while that corresponding to ideal frequency-division multiple-access (FDMA) systems has (k,l)th element[5]

$$[\mathbf{Q}(\omega)]_{k,l} = e^{j(\omega - 2\pi k)l/M}, \qquad 0 \le \omega \le \pi.$$

In contrast, for discrete Fourier transform (DFT) multiplexing, $\mathbf{Q}(\omega)$ is the DFT matrix,

[4]The superscript † denotes the conjugate-transpose operation.

[5]Note that $\mathbf{Q}(\omega)$ is both conjugate symmetric, *i.e.*, $\mathbf{Q}^*(\omega) = \mathbf{Q}(-\omega)$, and 2π-periodic.

i.e.,

$$[\mathbf{Q}(\omega)]_{k,l} = e^{-j2\pi kl/M}.$$

For Hadamard sequence based CDMA systems, for which we will develop a powerful generalization in Section II.3.1, we have

$$\mathbf{Q}(\omega) = \Xi,$$

where Ξ is the Hadamard matrix of appropriate dimension. Recall that the Hadamard matrix of dimension M, *viz.*, Ξ_M, where M is a power of two, is defined recursively: for $M = 2, 4, \ldots,$

$$\Xi_M = \frac{1}{\sqrt{2}} \begin{bmatrix} \Xi_{M/2} & \Xi_{M/2} \\ \Xi_{M/2} & -\Xi_{M/2} \end{bmatrix}$$

where $\Xi_1 = 1$.

CDMA system designers are frequently interested in the auto- and cross-correlation characteristics of the signature sequences. Indeed, the autocorrelation characteristics generally affect, for example, the ability of a receiver to synchronize to the transmission, while the cross-correlation characteristics generally affect the degree and nature of co-channel interference. Ideally, therefore, one would like the autocorrelation of each signature $h_k[n]$ to satisfy

$$h_k[n] * h_k[-n] \approx \delta[n], \tag{II.17}$$

and the cross-correlation between distinct signatures $h_k[n]$ and $h_l[n]$ to satisfy

$$h_k[n] * h_l[-n] \approx 0 \qquad k \neq l. \tag{II.18}$$

It is well-known that (II.17) and (II.18) are conflicting objectives for traditional signature sets (see, *e.g.*, Welch [21] or Sarwate and Pursley [12]). In fact, this is also true for spread-signature sets. To see this, let us define quadratic auto- or cross-correlation merit factors which penalize deviations from (II.17) and (II.18), respectively. Specifically, analogous to the merit factors defined by Golay [7], let

$$1/\mathcal{L}^h_{kl} = \frac{1}{2\pi} \int_{-\pi}^{\pi} [|H_k(\omega)\, H_l^*(\omega)| - \delta[k-l]]^2 \, d\omega. \tag{II.19}$$

Then, using (II.12), it is straightforward to verify that, for any $M \geq 2$,

$$\begin{aligned} \frac{1}{M^2} \sum_{k,l} \frac{1}{\mathcal{L}^h_{kl}} &= \frac{1}{2\pi M^2} \int_{-\pi}^{\pi} \left[\sum_k \left(|H_k(\omega)|^4 - 2|H_k(\omega)|^2 + 1 \right) + \sum_{k,\ l \neq k} \left(|H_k(\omega)|^2 |H_l(\omega)|^2 \right) \right] d\omega \\ &= \frac{1}{2\pi} \int_{-\pi}^{\pi} \frac{(M-1)}{M} \, d\omega = \frac{(M-1)}{M}. \end{aligned} \tag{II.20}$$

Hence, from (II.20) we see that good autocorrelation characteristics can only be obtained at the expense of cross correlation characteristics, and vice versa. At one extreme the trivial signature set corresponding to TDMA systems has perfect autocorrelation characteristics,

but the worst possible cross-correlation characteristics[6], *i.e.*,

$$\mathcal{L}_{kl}^{h} = \begin{cases} \infty & k = l \\ 1 & k \neq l \end{cases}.$$

At the opposite extreme we have the signature set corresponding to ideal FDMA systems. This set has perfect cross-correlation characteristics but poor autocorrelation characteristics; in particular,

$$\mathcal{L}_{kl}^{h} = \begin{cases} 1/(M-1) & k = l \\ \infty & k \neq l \end{cases}.$$

In practical CDMA systems, a compromise between these extremes is generally sought.

The auto- and cross-correlation characteristics constitute only one of the important issues in the design of good spread signature sets. For example, it is also important that the signature sets we develop are effective in spreading the transmission of each symbol of a user's transmission over a large range of time samples in order to mitigate the effects of fading. This is, of course, analogous to the objectives of spread-response precoding as developed in Part I. Accordingly, we define a dispersion factor $\mathcal{D}_h$ which measures a signature set's spreading capability via

$$\frac{1}{\mathcal{D}_h} = \frac{1}{M} \sum_m \frac{1}{\mathcal{D}_{h_m}}, \tag{II.21}$$

where $\mathcal{D}_{h_m}$ represents the dispersion in the sequence $h_m[n]$, *i.e.*,

$$\mathcal{D}_{h_m} = \left(\sum_m h_m^4[n] \right)^{-1}. \tag{II.22}$$

Note from (II.21) that, as we would expect from any reasonable definition of dispersion, the set has perfect spreading, *i.e.*, $\mathcal{D}_h \to \infty$, if and only if every signature in the set is perfectly spread, *i.e.*, $\mathcal{D}_{h_m} \to \infty$ for every $1 \leq m \leq M$.

Important insights are obtained by examining what values $\mathcal{D}_h$ can take. It is straightforward to verify, for instance, that for all orthonormal signature sets

$$\mathcal{D}_h \geq 1, \tag{II.23}$$

and that this bound is attained when $\mathbf{h}[n]$ is the TDMA signature set. More importantly, at another extreme we have, for finite-spread signature sets with temporal spread N,

$$\mathcal{D}_h \leq N, \tag{II.24}$$

with equality precisely when, for each $1 \leq m \leq M$,

$$|h_m[n]| = 1/\sqrt{N}, \qquad 0 \leq n \leq N-1.$$

[6]In fact, as can be verified from (II.19) and (II.20), this is true for any orthogonal signature set whose sequences have allpass Fourier transforms.

Hence, for finite-spread signature sets, maximum dispersion is achieved when the signature sequences are antipodal (binary-valued). For this reason, we refer to the corresponding signature sets as "maximally-spread." Note, too, that because they are discrete-valued, maximally-spread signature sets are especially attractive in terms of computational efficiency and numerical stability.

As another important design issue, it will also be important that the spread-signature sets we use possess what we refer to as a good "partitioning" characteristics. In particular, as we will see, good partitioning results in more uniform distribution of co-channel interference among users in the system. To develop this concept, we define the following modified correlation function

$$\Theta_{h_i}[n,m] = \sum_k h_i[n-Mk]\, h_i[m-Mk] \tag{II.25}$$

which corresponds to correlating $h_i[n]$ with a version of $h_i[n]$ in which all but every Mth sample is replaced with zero. While the complementarity condition (II.8) directly implies that

$$\sum_i \Theta_{h_i}[n,m] = \delta[n-m], \tag{II.26}$$

this condition says nothing about the properties of each of the M terms in the summation of (II.26). However, as will become apparent in Section II.4, the set has good partitioning characteristics when the unit-sample in (II.26) is, in some sense, distributed uniformly among the M modified correlation functions.

To make the notion of good partitioning characteristics more precise, we let

$$\tilde{\Theta}_{h_i}[n,m] = \Theta_{h_i}[n,m] - \frac{1}{M}\delta[n-m] \tag{II.27}$$

denote the deviation from ideal partitioning in each component. It is straightforward to show that $\tilde{\Theta}_{h_i}[n,m]$ is the following symmetry, periodicity, and finite energy characteristics:

$$\tilde{\Theta}_{h_i}[n,m] = \tilde{\Theta}_{h_i}[m,n], \tag{II.28a}$$

$$\tilde{\Theta}_{h_i}[n,m] = \tilde{\Theta}_{h_i}[n+kM, m+kM], \qquad \text{any } k, \tag{II.28b}$$

and

$$1/M^2 \le \sum_n \tilde{\Theta}^2_{h_i}[n,m] \le (1-1/M)^2. \tag{II.28c}$$

A signature set has asymptotically perfect partioning if $\tilde{\Theta}_{h_i}[n,m]$ can be made arbitrarily small using sufficiently long signatures. Accordingly, we define the following *partitioning factor:*

$$\frac{1}{\chi_h} = \frac{1}{M}\sum_i \frac{1}{\chi_{h_i}} \tag{II.29}$$

where

$$\frac{1}{\chi_{h_i}} = \sup_m \sum_n \tilde{\Theta}^4_{h_i}[n,m], \tag{II.30}$$

and note that good partitioning corresponds to large partitioning factors, and vice versa. It is important to note, however, that signature sets with good dispersion factors do not

necessarily have good partitioning characteristics[7]. Nevertheless, we emphasize that we shall be primarily interested in signature sets which have both good dispersion and good partitioning characteristics.

II.3.1 An Optimum Class of Spread-Signature Sets

In this section, we develop a family of orthogonal signature sets that are optimal in the sense of being maximally-spread, *i.e.*, having the best dispersion characteristics for a given length (or, equivalently, delay) constraint. As we discussed earlier, the maximally-spread condition is achieved precisely when the signature sequences are binary-valued. The signatures we construct are conveniently obtained out of a powerful paraunitary generalization of the Hadamard matrix, and have a computationally efficient recursive synthesis that is attractive in terms of modem implementation.

Our construction is based on the polyphase decomposition of a signature set (II.13). In particular, we rephrase the problem of designing a suitable orthogonal signature set $\mathbf{H}(\omega)$ into problem of designing a suitable paraunitary polyphase matrix $\mathbf{Q}(\omega)$. Thus, requiring that the desired $\mathbf{H}(\omega)$ correspond to a maximally-spread signature set is equivalent to requiring that polyphase matrix sequence $\mathbf{q}[n]$ whose transform is $\mathbf{Q}(\omega)$ be binary-valued.

We begin by observing that the Hadamard matrix Ξ is one matrix satisfying these properties. Accordingly, we let our zero-th order polyphase matrix be[8]

$$\mathbf{Q}^{(0)}(\omega) = \Xi, \tag{II.31}$$

and note that the spread of the corresponding signature set is $N = M$.

To obtain signature sets for which $N > M$, we exploit a recursion that preserves the binary sequence requirement; specifically, we let

$$\mathbf{Q}^{(i)}(\omega) = \Xi\, \mathbf{\Lambda}(M^{i-1}\omega)\, \mathbf{Q}^{(i-1)}(\omega), \qquad i = 1, 2, \ldots \tag{II.32}$$

where $\mathbf{\Lambda}(\omega)$ is the diagonal delay matrix whose diagonal is constructed from the elements of $\mathbf{\Delta}(\omega)$, *i.e.*, with $\mathbf{\Delta}(\omega)$ as defined in (II.15),

$$\mathbf{\Lambda}(\omega) = \operatorname{diag} \mathbf{\Delta}(\omega).$$

We see immediately that the paraunitary property (II.16) is preserved by the recursion (II.32) because the product of paraunitary matrices is also paraunitary. It is similarly straightforward to verify that the recursion (II.32) preserves binary sequence property—

[7]To verify this, it suffices to note that from any orthogonal signature set $h_m[n]$, we can construct a new orthogonal signature set $g_m[n]$ via

$$g_m[n] = \sum_k e_m[k]\, h_m[n - kM]$$

where the $e_m[n]$ are any set of nontrivial lossless (allpass) filters. However, while this new system generally has greater dispersion $\mathcal{D}_g > \mathcal{D}_h$, it is straightforward to show that the partitioning factor is unchanged, *i.e.*, $\chi_g = \chi_h$.

[8]For convenience, we restrict our attention to orders M for which Hadamard matrices exist. These include, for example, all integers M that are powers of two.

indeed, in the time domain one can interpret (II.32) and (II.31) as implementing a succession of simple sequence concatenations initiated with Hadamard sequences.

Using (II.13), we can also express the recursion (II.32) directly in terms of the signature set vector Fourier transform; specifically, we have, for $i = 1, 2, \ldots$,

$$\mathbf{H}^{(i)}(\omega) = \Xi \, \mathbf{\Lambda}(M^i \omega) \, \mathbf{H}^{(i-1)}(\omega). \tag{II.33}$$

From (II.33) we can verify that the spread of the signature set grows by a factor of M with each application of the recursion, so that, in particular, $\mathbf{H}^{(i)}$ has spread $N = M^{i+1}$ for $i = 0, 1, 2, \ldots$. For convenience, several sets of signature sequences obtained by the recursion (II.32) with (II.31), and corresponding to different values of M and N, are tabulated in Appendix III.C.

As a historical aside, it is interesting to note that orthogonal systems of the type constructed in this section have been reinvented numerous times over the last several decades, particularly for the case corresponding to $M = 2$. However, it would appear that this work is the first to attempt to exploit such systems in multiuser communication problems.

Using a variety of constructions, such systems emerged independently in a variety of unrelated communities within mathematics, physics, and engineering. Work within the engineering community dates traced back to 1950 when Golay constructed pairs of pseudorandom sequences which he referred to as "complementary sequences" [22] [23]. These sequences—now frequently referred to as Golay sequences—were defined as binary-valued sequences satisfying the frequency-domain complementarity condition (II.12) for $M = 2$.[9] These Golay sequences have subsequently been explored extensively, though the focus has been primarily on issues of existence of such pairs for various values of N; see, *e.g.*, [24] and [25].

From (II.12) it is apparent that binary-valued orthogonal sequences are a subset of complementary sequences. However, more importantly, complementary sequences also useful in the construction of orthogonal sequences, which both Golay and Turyn [26], and later Taki, *et al.* [27] observed in the case[10] $M = 2$. The corresponding generalizations for $M > 2$ appear in, *e.g.*, Tseng and Liu [28].

Within the mathematics community, binary-valued, pseudorandom, orthogonal sequence pairs (and, in particular, a time-domain version of the recursion (II.33) for $M = 2$) were also discovered independently by both Shapiro [29] and, later, Rudin[30]. As a result, the frequency domain representations for such sequences are sometimes referred to as Rudin-Shapiro polynomials.

As discussed in, *e.g.*, Odlyzko [31], several useful properties of such sequences, as well as their connections to other families of binary pseudorandom sequences, have been developed.

---

[9] As such, there is a natural correspondence between such complementary pairs and power complementary filters as developed in the multirate signal processing literature [19].

[10] To see this, it suffices to verify using (II.16) with (II.12) that

$$\mathbf{Q}(\omega) = \begin{bmatrix} A(\omega) & B(\omega) \\ B^*(\omega) & -A^*(\omega) \end{bmatrix} \tag{II.34}$$

is a paraunitary matrix whenever the corresponding sequences $a[n]$ and $b[n]$ constitute a complementary pair.

For example, the asymptotic auto- and cross-correlation characteristics of our maximally-spread orthogonal signature sets for the case $M = 2$ follow immediately from the results of Newman and Byrnes [32]. In particular, we have that

$$\mathcal{L}_{kk}^{h} \to 3, \qquad N \to \infty, \tag{II.35}$$

which, using (II.20), implies that for $k \neq l$,

$$\mathcal{L}_{kl}^{h} \to 3/2, \qquad N \to \infty. \tag{II.36}$$

Based on earlier discussion in Section II.3, (II.35) and (II.36) suggest that our maximally-spread signature sets are localized in neither time nor frequency. In fact, not only is this the case, but such strong spreading in *both* time and frequency is critical to good performance in our intended application. Furthermore, in addition to their good spreading characteristics, our maximally-spread signature sets have good asymptotic partitioning characteristics as well; specifically, $\chi_h \to \infty$ as $N \to \infty$.

II.4 System Characteristics

In this section, we develop the key characteristics of spread-signature CDMA systems, and then apply these results in developing efficient receivers for such systems. We begin with a general discussion of transmission characteristics.

II.4.1 Transmission Characteristics

Spread-signature CDMA systems give rise to transmissions with some rather special spectral and temporal characteristics, only some of which are shared by conventional CDMA systems. To illustrate the spectral features, we begin by observing from (II.1) that, provided the coded symbol stream of the mth user is stationary, the corresponding transmitted stream is cyclostationary with a time-averaged power spectrum given by

$$S_{y_m}(\omega) = |H_m(\omega)|^2 \, S_{x_m}(M\omega)/M,$$

where $S_{x_m}(\omega)$ is the power spectrum of the coded symbols of the mth user. When $x_m[n]$ consists of uncorrelated symbols of energy $\mathcal{E}_m$, as we shall generally assume in practice, the transmitted power spectrum associated with the mth user further simplifies to

$$S_{y_m}(\omega) = |H_m(\omega)|^2 \, \mathcal{E}_m/M. \tag{II.37}$$

From (II.37) several observations can be made. First, we immediately note that since $H_m(\omega)$ has unit-energy the total transmitted power in this case is $\mathcal{E}_m/M$. When compared with (II.3) we see that this appropriately results in a signal-to-noise ratio (SNR) that decreases inversely with system bandwidth.

We also note from (II.37) that, in general, the transmitted power spectrum, is not, strictly-speaking, white. However, when the maximally-spread signature sets of Section II.3.1 are used, the transmitted power spectrum is broadband and, in a particular sense, asymptotically white. More specifically, as $N \to \infty$, each $H_m(\omega)$ "converges" to a highly irregular

function whose energy is *effectively* uniformly-distributed over frequency. Furthermore, the transmitted spectrum corresponding to forward link transmission is typically truly white. Indeed, when the component coded symbol streams are mutually uncorrelated and of equal energy $\mathcal{E}_m = \mathcal{E}$, it is straightforward to verify using (II.12) that the aggregate transmitted power spectrum is

$$S_y(\omega) = \mathcal{E}, \tag{II.38}$$

where $y[n]$ is the aggregate transmission, *i.e.*,

$$y[n] = \sum_m y_m[n]. \tag{II.39}$$

The temporal characteristics of spread-signature CDMA transmissions are noteworthy as well. In traditional CDMA systems the individual (baseband) transmissions are generally binary-valued. However, in spread-signature CDMA systems, although the signature sequences and coded streams may be binary-valued (if, *e.g.*, the signature sequences of Section II.3.1 are used), the transmitted streams generated via the modulation (II.1) generally are not. This is, of course, a consequence of the overlap between modulated symbols than invariably results from choosing signature sequence lengths N that exceed the intersymbol epoch M. In fact, as $N \to \infty$, a simple Central Limit Theorem argument suggests that each $y_m[n]$ is a marginally Gaussian process.

This quasi-Gaussian behavior is generally rather appealing from the point of view of certain transmission security and capacity considerations. However, it is important to point out that, as was true in the case of spread-response precoding systems, these characteristics also pose significant engineering challenges in terms of managing peak-to-average power and receiver synchronization requirements. While such issues certainly warrant further investigation, they are beyond the scope of the present report.

II.4.2 Receiver Characteristics and Design

In Section II.4.1 we explored the transmission characteristics of spread-signature CDMA by examining what the coded symbol streams look like (after modulation) from the perspective of the channel. In this section, we develop efficient receivers for such systems by examining what the channel looks like from the perspective of the coded symbol stream (before modulation).

We begin by observing that what the coded symbol stream, in effect, "sees" is the cumulative effect of modulation, followed by distortion introduced by the channel, followed by processing performed at the receiver. Accordingly, we refer to what the coded symbol stream sees, then, as the "composite channel."

Before we explore the key properties of this composite channel, we must first develop an appropriate receiver structure for these systems. In general, the receiver processing required to recover the mth transmitted message is comprised of three stages. First, the received data $r[n]$ is equalized according to

$$\hat{y}_m[n] = \sum_k b_m[n;k]\, r[n-k]. \tag{II.40}$$

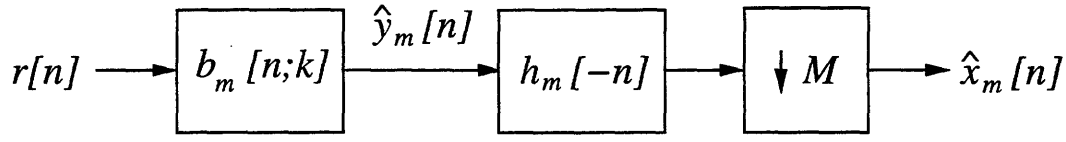

Figure II.3: *Receiver structure for extracting the symbol stream of the mth user. The first stage is equalization, producing $\hat{y}_m[n]$, while the second stage is demodulation, producing $\hat{x}_m[n]$. A final stage (not shown) is decoding.*

As is apparent from (II.40) and as is depicted in Fig. II.3, the corresponding equalizer is, in general, a linear time-varying filter whose kernel we denote by $b_m[n;k]$. Because the fading channel coefficients and statistics are assumed to be available to the receiver, the equalizer kernel $b_m[\cdot\,;\cdot]$ is generally a function of all the channel kernels $a_k[\cdot\,;\cdot]$, $k = 1, 2, \ldots M$, although the dependence is often simpler in certain special cases of interest.

In the second stage, also depicted in Fig. II.3, the equalized data is demodulated from the corresponding signature sequence, *viz.*,

$$\hat{x}_m[n] = \sum_k \hat{y}_m[k]\, h_m[k - Mn].$$

This is conveniently interpreted as a discrete-time matched-filter and downsample operation.

Finally, the last stage of the message recovery, which is not depicted in Fig. II.3, consists of decoding the demodulated stream $\hat{x}_m[n]$ (using, for example, maximum likelihood methods). It is important to point out, however, that while we will not consider the actual implementation of the decoder in this report, we will discuss in Section II.5 what kinds of coding and decoding strategies are appropriate for spread-signature CDMA, and their effect on system performance.

The composite system consisting of modulation, the channel, equalization, and demodulation has some appealing characteristics provided the channel, and, in turn, the corresponding equalizers, have some reasonable ergodicity properties. In effect, these ergodic properties are required to ensure that spreading the transmission of each symbol over a sufficiently long time interval by modulation allows these symbols to see the average characteristics of the fading channel—*i.e.*, that the time-averaging implicit in the modulation is equivalent to ensemble-averaging. The following technical definition will prove to be sufficient for our purposes.

Definition 2 *Let $f_j[n;k]$ be the kernels of a family of linear systems, and define*

$$\tilde{f}_j[n;k] = f_j[n;k] - E\left[f_j[n;k]\right]. \tag{II.41}$$

Furthermore, let

$$d_j^{j'}[n,m;k,l] = \tilde{f}_j[n;k]\, \tilde{f}_{j'}^{*}[m;l] \tag{II.42}$$

and define

$$\tilde{d}_j^{j'}[n,m;k,l] = d_j^{j'}[n,m;k,l] - E\left[d_j^{j'}[n,m;k,l]\right]. \tag{II.43}$$

Then the family $f_j[n;k]$ *is* admissibly ergodic *if the following conditions are satisfied:*

$$E\left[f_j[n;k]\right] = E\left[F_j\right]\delta[k] \tag{II.44a}$$

$$E\left[\tilde{f}_j[n;k]\,\tilde{f}^*_{j'}[m;l]\right] = R^{j'}_j[n-m;k]\,\delta[k-l] \tag{II.44b}$$

$$E\left[\tilde{d}^{j'}_j[n,m;k,l]\,\tilde{d}^{j'*}_j[n',m';k',l']\right] = T^{j'}_j[n-m,n'-m',n-n';k,l,k',l'] \tag{II.44c}$$

$$S_{R^{j'}_j} = \sum_n \sum_k \left|R^{j'}_j[n;k]\right| < \infty \tag{II.44d}$$

$$S_{T^{j'}_j} = \sum_{\substack{n_1,n_2\\n_3}} \sum_{\substack{k_1,k_2\\k_3,k_4}} \left|T^{j'}_j[n_1,n_2,n_3;k_1,k_2,k_3,k_4]\right| < \infty \tag{II.44e}$$

Definition 2, in fact, represents a straightforward generalization of the corresponding definitions constructed in Part I. In particular, conditions (II.44a), (II.44b) and (II.44c) are essentially stationarity constraints, while (II.44d) and (II.44e) are ergodicity constraints. Note, too, that for convenience we have omitted specification of the frequency ω and time n from $E\left[F_j(\omega;n)\right]$ in (II.44a) due to stationarity.

The key properties of the composite channels, which we now develop, represent a natural generalization of those developed for single-user systems in Part I. In particular, we show that subject to only relatively mild ergodicity constraints, the use of spread-signature modulation with sufficiently long signatures leads to composite channels that are effectively a collection of uncorrelated additive white noise channels, each of which is not only free of fading, but has no intersymbol interference. In developing our detailed results, we consider the forward link and reverse link systems separately since there are some fundamental differences in behavior.

The Forward Link

The characteristics of the composite system for the forward link are summarized in the following theorem. A proof is provided in Appendix III.D.

Theorem 2 (Forward Link) *Let* $x_m[n]$ *be mutually uncorrelated sequences of zero-mean, uncorrelated symbols, each with energy* $\mathcal{E}_m$*, and let* $a_m[n;k]$ *and* $w[n]$ *be as defined in (II.2) and (II.4). Furthermore, let the common equalizer be*

$$b_1[n;k] = b_2[n;k] = \cdots = b_M[n;k] \triangleq b[n;k],$$

and let $c[n;k]$ *denote the kernel of the linear system formed by cascading the channel whose kernel is* $a[n;k]$*, with the equalizer whose kernel is* $b[n;k]$*, i.e.,*

$$c[n;k] = \sum_l b[n;l]\,a[n-l;k-l]. \tag{II.45}$$

Finally, suppose the $c[n;k]$ and $b[n;k]$ are both admissibly ergodic kernels in the sense of Definition 2. Then, as $\mathcal{D}_h \to \infty$ (infinite dispersion) and $\chi_h \to \infty$ (perfect partitioning[11]), we have, for each n,

$$\hat{x}_m[n] \xrightarrow{\text{m.s.}} E[C]\, x_m[n] + v_m[n], \tag{II.46}$$

where the $v_m[n]$ are mutually uncorrelated, zero-mean, complex-valued, marginally Gaussian white noise sequences that are uncorrelated with the input symbol sequences $x_m[n]$. Furthermore, the variance of the noise $v_m[n]$ is independent of both m and n, and is given by

$$\operatorname{var} v_m[n] = \mathcal{N}_0 \mathcal{W}_0 E\left[|B|^2\right] + \operatorname{var}[C]\bar{\mathcal{E}}, \tag{II.47}$$

where

$$\bar{\mathcal{E}} = \frac{1}{M}\sum_{k=1}^{M} \mathcal{E}_k \tag{II.48}$$

is the average transmitted power. In both (II.46) and (II.47) we have, for convenience, again omitted specification of the time sample n and frequency ω corresponding to B and C due to stationarity.

While we postpone more general remarks until Section II.4.2, we emphasize that Theorem 2 implies that the composite forward link channels are asymptotically mutually uncorrelated, identical, nonfading, quasi-Gaussian channels with no intersymbol interference. Moreover, from Theorem 2 we also note that the SNR on the mth of these composite channels is

$$\gamma_m = \frac{\mathcal{E}_m |E[C]|^2}{\mathcal{N}_0 \mathcal{W}_0 E[|B|^2] + \bar{\mathcal{E}} \operatorname{var}[C]}. \tag{II.49}$$

The design of a suitable equalizer for the receiver in this case is straightforward. In particular, for sufficiently slow fading we have

$$C(\omega;n] \approx A(\omega;n]\, B(\omega;n].$$

so that (II.49) becomes

$$\gamma_m = \frac{\mathcal{E}_m}{\bar{\mathcal{E}}} \left[\frac{|E[AB]|^2}{(\mathcal{N}_0 \mathcal{W}_0 / \bar{\mathcal{E}}) E[|B|^2] + \operatorname{var}[AB]} \right]. \tag{II.50}$$

Then, recognizing that the term in brackets in (II.50) is identical in form to an SNR expression that was maximized in Part I, we immediately deduce that (II.49) is maximized when

$$B(\omega;n] \propto \frac{A^*(\omega;n]}{1+\bar{\alpha}}, \tag{II.51}$$

where

$$\bar{\alpha}(\omega;n] = \frac{\bar{\mathcal{E}} |A(\omega;n]|^2}{\mathcal{N}_0 \mathcal{W}_0}. \tag{II.52}$$

[11] Actually, perfect partitioning is strictly speaking not required for the forward link theorem to hold, although this is not apparent in our proof. However, it is necessary for the reverse link theorem to hold.

Furthermore, in this case the corresponding SNR can be expressed as

$$\gamma_m = \frac{\mathcal{E}_m}{\bar{\mathcal{E}}} \left[\frac{1}{E\left[\frac{1}{1+\bar{\alpha}}\right]} - 1 \right], \tag{II.53}$$

which may be further simplified using methods used in Part I. In fact, as we will discuss further in Section II.5.1, when $\mathcal{E}_m = \bar{\mathcal{E}}$, these results specialize to precisely those obtained in Part I.

The Reverse Link

The following theorem summarizes the characteristics of the composite channel on the reverse link. We emphasize that in this scenario we are assuming completely uncoordinated (*i.e.*, fully asynchronous) transmissions from mobiles to the base. A proof is again provided in Appendix III.D.

Theorem 3 (Reverse Link) *Let $x_m[n]$ be mutually uncorrelated sequences of zero-mean, uncorrelated symbols, each with energy $\mathcal{E}_m$, and let $a_m[n;k]$ and $w[n]$ be as defined in (II.2) with the channel kernels being statistically independent. Furthermore, let $c_{mi}[n;k]$ denote the kernel of the linear system formed by cascading the channel seen by user m whose kernel is $a_m[n;k]$, with the equalizer corresponding to the detection of user i, whose kernel is $b_i[n;k]$, i.e.,*

$$c_{mi}[n;k] = \sum_l b_i[n;l]\, a_m[n-l;k-l]. \tag{II.54}$$

Finally, suppose the $c_{mi}[n;k]$ and $b_m[n;k]$ are admissibly ergodic kernels in the sense of Definition 2. Then, as $\mathcal{D}_h \to \infty$ (infinite dispersion) and $\chi_h \to \infty$ (perfect partitioning), we have, for each n,

$$\hat{x}_m[n] \xrightarrow{\text{m.s.}} E\left[C_{mm}\right] x_m[n] + v_m[n], \tag{II.55}$$

where the $v_m[n]$ are mutually uncorrelated, zero-mean, complex-valued, marginally Gaussian white noise sequences that are uncorrelated with the input symbol sequences $x_m[n]$. Furthermore, the variance of the noise samples $v_m[n]$ is independent of n and satisfies

$$\operatorname{var} v_m[n] = \mathcal{N}_0 \mathcal{W}_0 E\left[|B_m|^2\right] + \frac{1}{M} \sum_{k=1}^{M} \mathcal{E}_k \operatorname{var}\left[C_{km}\right]. \tag{II.56}$$

Again, in both (II.55) and (II.56) we have omitted specification of the time sample n and frequency ω corresponding to B_m and C_{km} due to stationarity.

Again, although we defer further more general remarks until Section II.4.2, we emphasize that, as in the forward link case, Theorem 3 implies that the composite reverse link channels are asymptotically mutually uncorrelated, nonfading quasi-Gaussian channels with no intersymbol interference.

From Theorem 3, we observe that the SNR of the composite channel seen by the mth user is

$$\gamma_m = \frac{\mathcal{E}_m |E[C_{mm}]|^2}{\mathcal{N}_0 \mathcal{W}_0 E\left[|B_m|^2\right] + \frac{1}{M}\sum_{k=1}^{M} \mathcal{E}_k \operatorname{var}[C_{km}]}. \tag{II.57}$$

As in the forward link, it is possible to develop equalizers yielding the best possible SNR in the composite channels for the reverse link. In particular, given sufficiently slow fading that

$$C_{kl}(\omega; n] \approx A_k(\omega; n]\, B_l(\omega; n],$$

we can re-express (II.57) in the form

$$\gamma_m(B_m) = \frac{\mathcal{E}_m |E[A_m\, B_m]|^2}{\mathcal{N}_0 \mathcal{W}_0 E\left[|B_m|^2\right] + \frac{1}{M}\sum_{k=1}^{M} \mathcal{E}_k \operatorname{var}(A_k\, B_m)}. \tag{II.58}$$

In turn, the following lemma directly establishes the optimum equalizer for the mth user, *viz.*,

$$B(\omega; n] \propto \frac{A_m^*(\omega; n]}{1 + \frac{1}{M}\sum_{k=1}^{M} \alpha_k(\omega; n]}, \tag{II.59}$$

where

$$\alpha_m(\omega; n] = \frac{\mathcal{E}_m |A_m(\omega; n]|^2}{\mathcal{N}_0 \mathcal{W}_0} \tag{II.60}$$

is the SNR at the receiver corresponding to the mth user. A proof of the lemma is provided in Appendix III.E.

Lemma 1 *Let $A_1, A_2, \ldots, A_M$ denote a collection of statistically-independent, complex-valued, zero-mean Gaussian random variables, each with finite variance, and let $\mathcal{N}_0\mathcal{W}_0$ and $\mathcal{E}_1, \mathcal{E}_2, \ldots, \mathcal{E}_M$ be arbitrary real, non-negative weights. Then the function $\gamma_m(B_m)$ defined in (II.58) satisfies*

$$\frac{\gamma_m(B_m)}{M} \leq \left(E\left[\frac{1 + \frac{1}{M}\sum_{k \neq m} \alpha_k}{1 + \frac{1}{M}\sum_{k} \alpha_k} \right] \right)^{-1} - 1 \tag{II.61}$$

where the α_k are as defined in (II.60). Furthermore, equality in (II.61) holds when

$$B \propto \frac{A_m^*}{1 + \frac{1}{M}\sum_{k=1}^{M} \alpha_k}.$$

General Remarks

Several aspects of both the interpretation and the implications of Theorems 2 and 3 are worth developing in more detail.

First, it is important to emphasize that these theorems do not establish that the composite channels are truly Gaussian channels. For example, although we argue that the additive noise sequence in the composite channel models is marginally Gaussian, we do not assert that these noise samples are actually jointly Gaussian. More generally, while these theorems describe the second-order properties of the composite channels, it should be stressed that they say very little about higher-order statistical dependencies.[12] Indeed, while they establish that the collection of noises and coded streams are mutually uncorrelated, there is no claim of full mutual independence. Nevertheless, as we will see in Section II.5, useful approximations are obtained by modeling the composite channel as truly Gaussian and thereby ignoring these residual statistical dependencies.

It is also useful to note that the additive noise in the composite channel model can be viewed as consisting of three components. Indeed, from both (II.47) and (II.56) we see that one component is due to the receiver noise in the original fading channel, while another is due to co-channel interference from other users. However, the third component is a form of self-interference generated as a by-product of the modulation, and thus the total noise power has a term that depends on the transmitted signal power. Collectively, these factors, in turn, give rise to the rather special equalizer structure which is optimum for such systems. In particular, we note that the optimum equalizers for these systems are minimum mean-square error type equalizers in contrast to the matched filter type equalizers associated with traditional CDMA systems.

It should also be emphasized that in establishing Theorems 2 and 3, both the dispersion and partitioning characteristics of the signature set are important, as the proofs of these theorems reveal. In particular, it is perfect dispersion that leads to the absence of fading and intersymbol interference in the composite channels, while it is perfect partitioning that leads to mutually uncorrelated, identical white noise characteristics in the composite channels.

In addition, while Theorems 2 and 3 establish asymptotic results which involve signature sequences having infinite temporal spread ($N \to \infty$), it is important to note that the asymptotic behavior can, in fact, be approximated arbitrarily closely with realizable, finite-spread signature sets. In fact, it this approximation property that underlies the practical importance of these theorems.

In general, the temporal spread required to achieve a given level of approximation to the results of the theorems depends on the coherence time characteristics of the fading. Specifically, analogous to the results for spread-response precoding, if N' is the spread required in the case of memoryless fading, then the spread required when the coherence time (in samples) is τ_a is

$$N = N'(\tau_a + 1).$$

Thus, a larger coherence time implies that greater delay must be incurred to achieve a given level of performance. This, of course, is true of communication over fading channels

[12] In fact, because of the emphasis on second-order properties, versions of these theorems hold even when the original channel noises and kernels are not Gaussian.

in general. However, it is important to recognize that the delay constraints in spread-signature CDMA are no worse than in other systems employing, for example, interleaving.

Although greater coherence times require longer signature sequences, it is important to note that the computational requirements need not grow with coherence time. In fact, the required number of *non-zero* coefficients in each signature sequence is independent of the coherence time. In particular, to match the coherence time characteristics of a channel of interest, it suffices to upsample some prototype set of signature sequences (such as those developed in Section II.3.1) to achieve the necessary temporal spread. Furthermore, we note that the energy, dispersion, partitioning, and computational characteristics are all unaffected by such upsampling.

While this upsampling approach to coherence time matching is also used with spread-response precoding, an important difference in the case of spread-signature CDMA is that the upsampling factor K cannot be freely chosen. In particular, in order to preserve orthogonality among the signatures, we may only upsample the signatures by an integer K that is not a multiple of a prime factor of the number of users M.[13] Hence, if the $h_m[n]$ are a set of prototype maximally-spread signature sequences applicable to memoryless fading, the signature sequences applicable when the coherence time is τ_a are given by

$$h_m^{(\tau_a)}[n] = \begin{cases} h_m[n/K_0] & n = \cdots, -K_0, 0, K_0, 2K_0, \cdots \\ 0 & \text{otherwise} \end{cases} \tag{II.62}$$

where K_0 denotes the smallest integer that is not less than $\tau_a + 1$ and is not a multiple of a prime factor of M.

II.5 Performance

In this section we explore both the effective capacity and bit-error rate characteristics of spread-signature CDMA systems. Again, we examine the forward and reverse links separately so as to emphasize some important differences between these cases.

II.5.1 The Forward Link

Due to the coordinated nature of the transmission, performance on the forward link generally follows immediately from the results presented for single-user systems in Part I. Indeed, on the forward link, it is typical to choose

$$\mathcal{E}_1 = \mathcal{E}_2 = \cdots = \mathcal{E}_M = \bar{\mathcal{E}} \triangleq \mathcal{E},$$

in which case the optimum equalizer (II.51) and the optimum SNR (II.53) both specialize to precisely those derived in the single-user scenario. Furthermore, since forward link performance for any M coincides with reverse link performance for $M = 1$, we will ultimately rederive these results as special cases in Section II.5.2.

[13] This implies, for instance, that when the number of users M is a power of two, *i.e.*, $M = 2^J$, we can use any odd K. Likewise, for $M = 3^J$, we can use any K which is not a multiple of 3, and for $M = 6^J$, we can use any K which is not a multiple of 2 or 3, *i.e.*, $K = 5, 7, 11, \ldots$, etc.

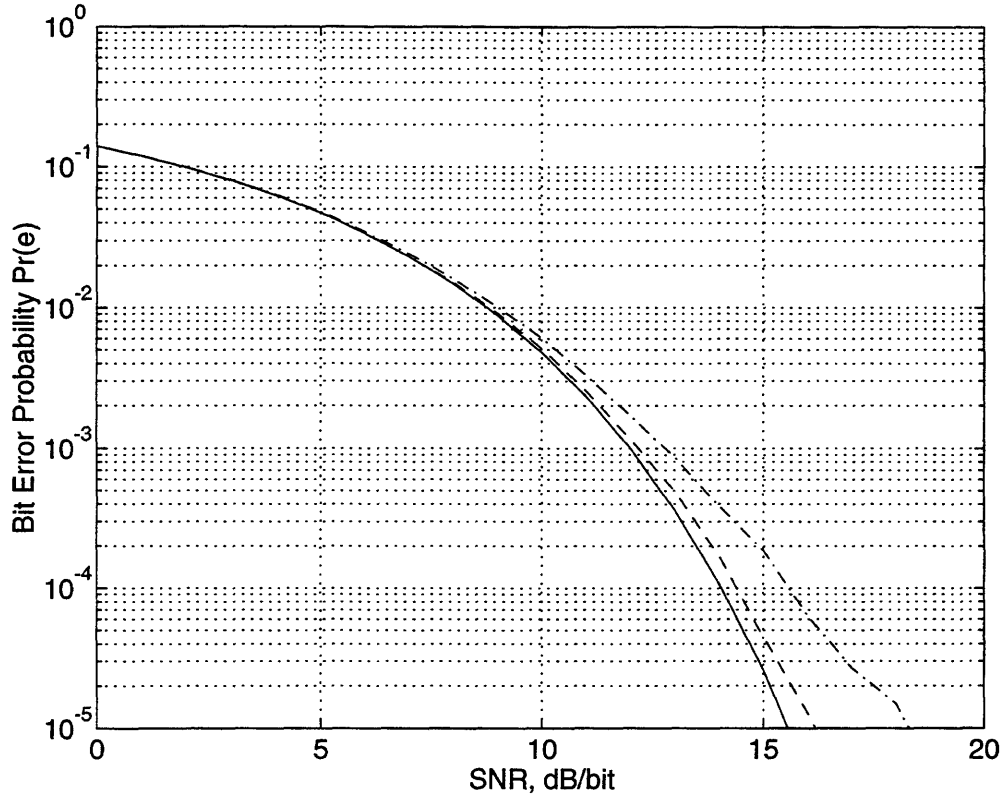

Figure II.4: *Bit error probabilities using uncoded QPSK in Rayleigh fading on the forward link. The dash-dotted and dashed curves represent the performance obtained using maximally-spread signature sets with $N' = 32$ and $N' = 128$, respectively. The solid line represents the ideal performance bound ($N' \to \infty$).*

While many of the performance characteristics on the forward link may be directly extracted from the corresponding results in Part I, those concerning performance with realizable (finite-spread) signature sets cannot. Accordingly, we depict forward link performance obtained with realizable signature sets in Fig. II.4. Specifically, we plot realizable uncoded quadrature phase-shift keying (QPSK) bit error rate performance in Rayleigh fading as a function of SNR per bit as measured through Monte Carlo simulations. In these simulations we use the maximally-spread signature sets of dimension $M = 2$ developed in Section II.3.1, and the dash-dotted and dashed curves indicate the performance corresponding to $N' = 32$ and $N' = 128$, respectively. For comparison, the solid curve corresponds to the asymptotic performance obtained with infinite temporal spread ($N' \to \infty$).

More generally, the single-user scenario ($M = 1$) warrants further discussion. As remarked earlier, no nontrivial finite-spread orthogonal signatures for $M = 1$ exist. As a result, in Part I the orthogonality (losslessness) constraint had to be relaxed in developing realizable precoders. In turn, this led to a corresponding degradation in the precoder performance. However, from within the broader framework of this report, we can see that

orthogonal signature sets corresponding to $M \geq 2$ can also be usefully applied to single-user precoding problems. In particular, we may distribute successive symbols in a stream $x[n]$ among M different substreams $x_m[n]$ by periodic subsampling, *i.e.*,

$$x_m[n] = x[nM + m - 1].$$

and then use an orthogonal spread signature set of order M to implement perfectly lossless precoding. At the receiver, the substreams may be demodulated from the signature sequences, and appropriately reintegrated into the single stream $\hat{x}[n]$.

This strategy for implementing lossless precoding has a conceptually rather useful interpretation. Specifically, the cyclic distribution of symbols among substreams may, itself, be interpreted as a lossless system, and, hence, in effect what we construct in this manner is a linear periodically time-varying precoder[14]. Hence, we see that by adopting this more general precoder structure we are able to achieve lossless spread-response precoding with finite-length filters.

In light of these observations, we see that the curves in Fig. II.4 also correspond to the single-user performance that is achievable using the improved precoders. And, comparing Fig. II.4 to Fig. I.5, we see that significantly better performance is achieved for a given length constraint (N') when we have perfect orthogonality (losslessness).

II.5.2 The Reverse Link

The performance characteristics on the reverse link are dramatically different than those on the forward link due the the uncoordinated nature of the transmissions, as we now illustrate. We begin by noting that, in practice, on the reverse link power control is generally employed to adjust the transmitter power for each user so that the average received power from each user is the same, *i.e.*, for all users m, the SNR in the corresponding original channel is

$$E\left[\alpha_m(\omega; n]\right] \triangleq 1/\zeta_0. \tag{II.63}$$

where $\alpha_m(\omega; n]$ is as defined in (II.60). Indeed, such power control is a practical technique for mitigating the vulnerability of CDMA systems to, among other problems, near-far effects [18].

Some important insights into the potential capacity of spread-signature CDMA systems arise out of the theorems of Section II.4.2. Theorem 3, in particular, suggests that the composite quasi-Gaussian channel seen by the mth user has a "capacity" given by

$$\mathcal{C}_m = \mathcal{W}_0 \log(1 + \gamma_m) \tag{II.64}$$

where γ_m is the SNR in the composite channel of the mth user. However, we emphasize that caution must be exercised in interpreting this notion of capacity. In particular, we note that this measure of capacity ignores all statistical effects of greater than second order in the composite channels—despite the fact that such effects can in principle be exploited to

[14]We remark as an aside that traditional interleavers are essentially trivial examples of such linear periodically time-varying systems.

yield still higher throughputs. Nevertheless, the particular concept of constrained capacity defined here has a useful interpretation as we will develop. In particular, it provides a measure of throughput that can be achieved when traditional forms of coding are superimposed on our CDMA system.

Convenient expressions can be obtained for the composite channel SNR which maximizes this effective capacity. In particular, from Lemma 1, we have that when we use optimum equalization, γ_m can be expressed as

$$\frac{\gamma_m}{M} = \frac{1}{\beta_m} - 1, \tag{II.65}$$

where

$$\beta_m = E\left[\frac{1 + \frac{1}{M}\sum_{k\neq m}\alpha_k}{1 + \frac{1}{M}\sum_{k}\alpha_k}\right]. \tag{II.66}$$

Under our power control assumption, β_m as defined in (II.66) is independent of m, and thus we simply use β_0, γ_0, and $\mathcal{C}$ to denote the quantities (II.65), (II.66), and (II.64) respectively. Furthermore, in this case, by exploiting symmetry (II.66) can be expressed in closed form in terms of the exponential integral. In particular, we have the following Lemma, whose proof is provided in Appendix III.F.

Lemma 2 *Let $v_1, v_2, \ldots, v_M$ be independent, identically-distributed exponential random variables with mean $1/\mu$. Then for any $1 \leq m \leq M$,*

$$E\left[\frac{1 + \sum_{k\neq m} v_k}{1 + \sum_{k} v_k}\right] = \frac{M-1}{M} + \frac{\mu^M}{M!}\left[(-1)^{M+1}e^{\mu}E_1(\mu) + \sum_{k=0}^{M-2}(-1)^{M-k}\frac{k!}{\mu^{k+1}}\right], \tag{II.67}$$

where

$$E_1(\nu) = \int_{\nu}^{\infty}\frac{e^{-t}}{t}\,dt. \tag{II.68}$$

is the exponential integral [15].

Thus, using Lemma 2 with $v_k = \alpha_k/M$ we immediately obtain that (II.66) can be expressed as

$$\beta_0 = \frac{M-1}{M} + \frac{(M\zeta_0)^M}{M!}\left[(-1)^{M+1}e^{M\zeta_0}E_1(M\zeta_0) + \sum_{k=0}^{M-2}(-1)^{M-k}\frac{k!}{(M\zeta_0)^{k+1}}\right]. \tag{II.69}$$

Hence, evaluating (II.64) via (II.65) and (II.69), we obtain relationships for the capacity per user as a function of the number of users M, the SNR, and the bandwidth per user. In Fig. II.5 we plot capacity per user as a function of M at various levels of SNR, while in Fig. II.6 we plot capacity per user as a function of SNR for various values of M, with the Gaussian channel capacity included for comparison.

Note from Fig. II.6 that for $M \geq 2$ the reverse link capacity appears to saturate at

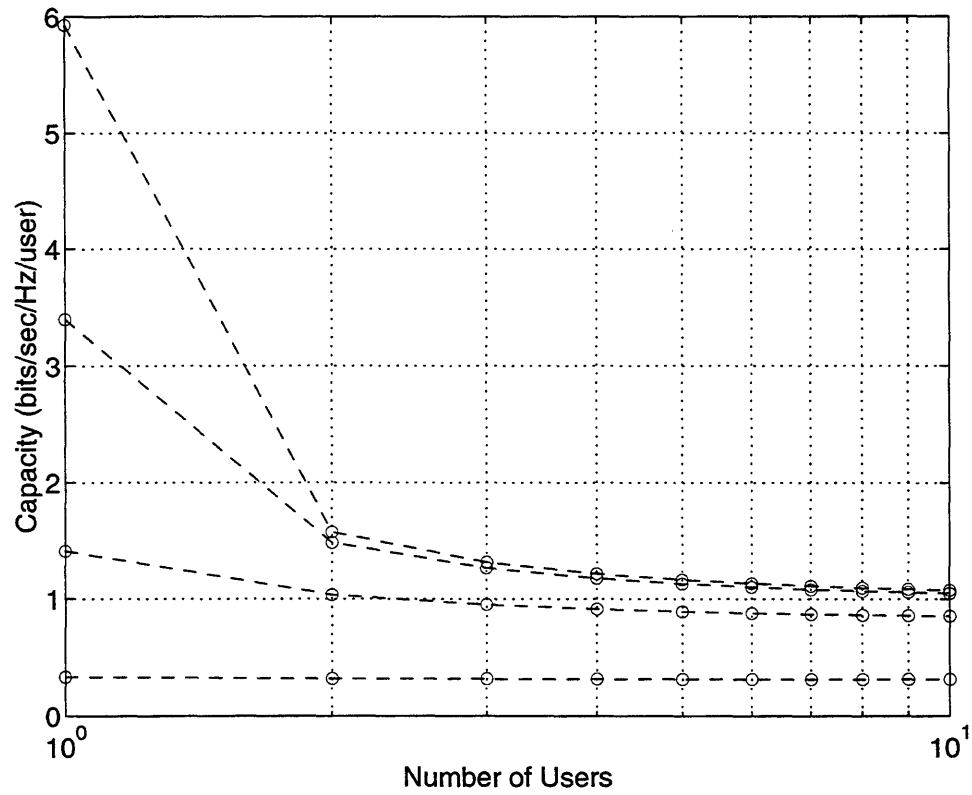

Figure II.5: *Reverse link capacity per user as a function of the number of users M. The successively higher curves correspond to SNRs of -5, 5, 15, and 25 dB. Note that the capacities corresponding to $M = 1$ also coincide with forward link performance with any number of users. The connecting dashed lines have no special interpretation; they are provided as visual aides only.*

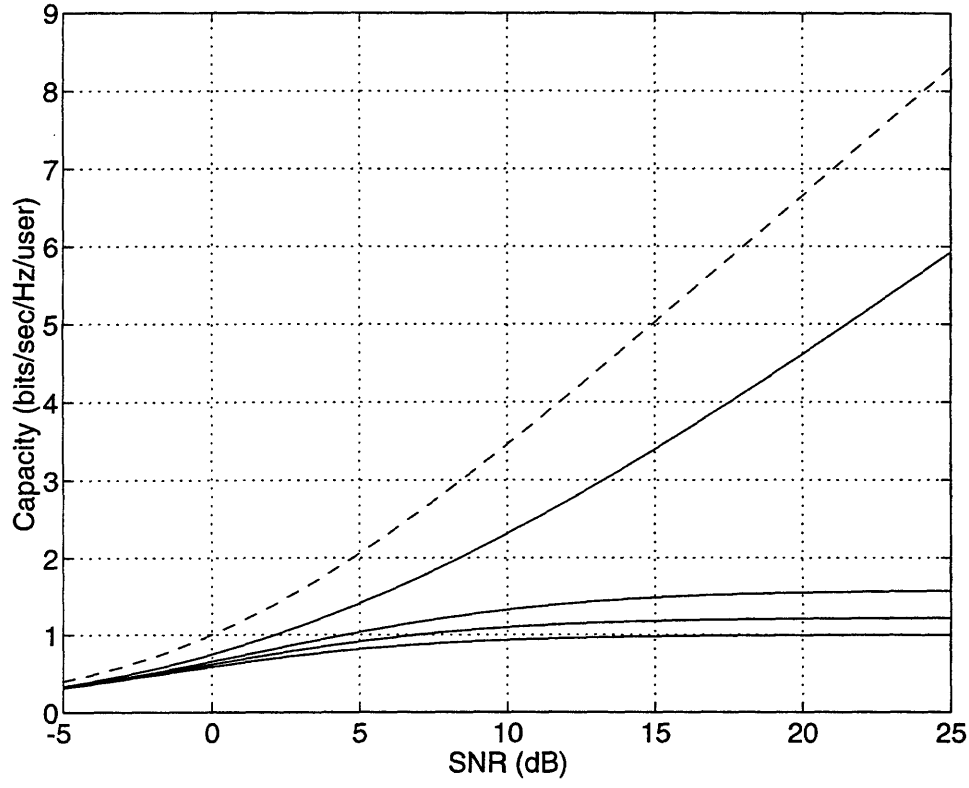

Figure II.6: *Capacity per user as a function of SNR. The successively lower solid curves correspond to reverse link transmission with $M = 1$, $M = 2$, $M = 4$, and $M \to \infty$ users. Note that the curve for $M = 1$ also coincides with forward link capacity with any number of users. The dashed line indicates the capacity of the corresponding Gaussian channel.*

high SNR, with the saturation level depending on the number of users. This is, in fact, the case, and it reflects the fact that reverse link performance is fundamentally interference limited rather than noise limited. This phenomenon, which is a direct consequence of the constrained receiver structure we employ, is well known; see, *e.g.*, Verdu [33]. While it is possible to design multiple-access systems that are strictly noise limited, this requires the use of receivers employing joint detection strategies. Unfortunately, joint detection is, in general, computationally very intensive, particularly when the number of users in the system is large [34]. For these reasons, such receivers are often considered impractical.

To verify the interference-limited behavior, let us consider the high SNR regime performance in more detail. In this case, we may use the series expansion [15]

$$E_1(\nu) = -\Gamma_0 - \ln\nu - \sum_{k=1}^{\infty} \frac{(-1)^k \nu^k}{k\, k!}, \tag{II.70}$$

with $\Gamma_0 = 0.57721\cdots$ denoting Euler's constant, to show that at high SNR ($\zeta_0 \to 0$), (II.69) satisfies

$$\beta_0 \to \frac{M-1}{M}. \tag{II.71}$$

Thus the asymptotic capacity on the reverse link in this regime is

$$\mathcal{C} \sim \log\left(\frac{2M-1}{M-1}\right). \tag{II.72}$$

Hence, (II.72) implies that the resulting capacity is finite, consistent with the saturation behavior apparent in Fig. II.6.

Another important asymptotic regime to explore is the large number of user scenario. Fortunately, as $M \to \infty$, convenient closed form expressions are possible. In particular, since the α_k are independent, identically-distributed random variables, we have, by the law of large numbers

$$\frac{1}{M}\sum_{k=1}^{M} \alpha_k \to 1/\zeta_0 \qquad \text{as } M \to \infty.$$

Hence, we get

$$\gamma_0 \to \frac{1}{1+\zeta_0} \tag{II.73}$$

and, in turn, (II.64) becomes

$$\mathcal{C} \to \mathcal{W}_0 \log\left(\frac{2+\zeta_0}{1+\zeta_0}\right). \tag{II.74}$$

Note from (II.74) that when the system contains large numbers of users, we have, regardless of the transmitter power used, $\mathcal{C}/\mathcal{W}_0 < 1$ bit/sec/Hz with $\mathcal{C}/\mathcal{W}_0 \to 1$ bit/sec/Hz as $\zeta_0 \to 0$.

It is also significant that in this case, the equalizer structure simplifies substantially as well. Again, via the law of large numbers we get

$$B \propto A_m^*, \tag{II.75}$$

the familiar matched filter equalizer, which we note is substantially easier to implement than

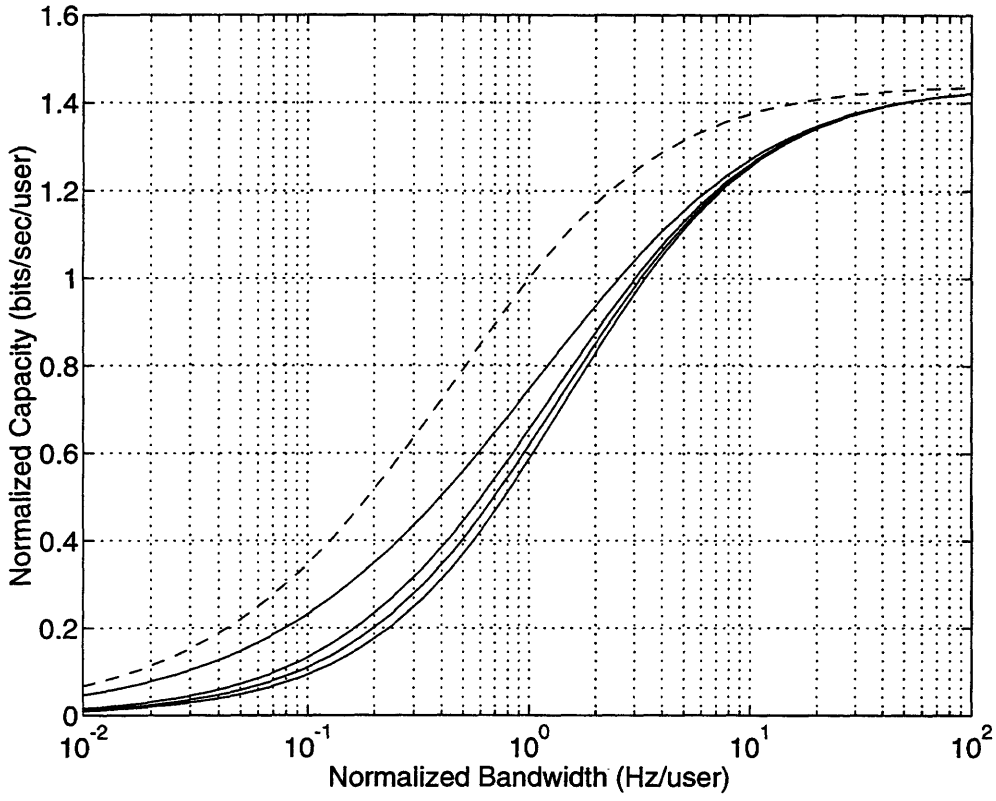

Figure II.7: *Capacity per user as a function of bandwidth. The successively lower solid curves correspond to reverse link transmission with $M = 1$, $M = 2$, $M = 4$, and $M \to \infty$ users, respectively. Note that the $M = 1$ curve for the reverse link coincides the performance of the forward link with any number of users. The dashed line corresponds to the capacity of the Gaussian channel.*

the optimum equalizer for finite M. Fortunately, the asymptotic performance is achieved for fairly moderate values of M as Fig. II.5 reveals, so that in practice this simpler equalizer can frequently be used.

Let us now turn our attention to the SNR-limited setting, and consider the large bandwidth behavior. In Fig. II.7 we plot normalized capacity as a function of bandwidth per user for various values of M, with the Gaussian channel capacity included for comparison. Several general remarks regarding Fig. II.7 are appropriate. First, as in the case of the Gaussian channel, the capacity in our multiuser fading environment increases monotonically with bandwidth per user. Second, the horizontal distance between the $M = 1$ and $M \geq 2$ curves quantifies how much additional bandwidth is required to compensate for the absence of coordination on the reverse link.

Perhaps the most important observation from Fig. II.7, however, is that the infinite bandwidth capacity is identical to that of the Gaussian channel. To verify this property,

we note that using the asymptotic series expansion [15]

$$E_1(\nu) = e^{-\nu} \sum_{k=0}^{\infty} (-1)^k \frac{k!}{\nu^{k+1}}, \quad \text{large } \nu, \tag{II.76}$$

we have that for large $\mathcal{W}_0$ (*i.e.*, large ζ_0),

$$\beta_0 \sim 1 + \sum_{k=0}^{\infty} \frac{(k+M)!}{M!} \frac{(-1)^{k+1}}{(M\zeta_0)^{k+1}}. \tag{II.77}$$

Using (II.77) in (II.65), we see that for large $\mathcal{W}_0$,

$$\gamma_0 \sim \frac{M}{M\zeta_0 - 1} \tag{II.78}$$

However, since γ_0 in (II.78) is small, (II.64) can be expressed asymptotically as

$$\mathcal{C} \sim \mathcal{W}_0 \gamma_0 = \frac{M\mathcal{W}_0}{M\zeta_0 - 1}. \tag{II.79}$$

Using the fact that (II.60) and (II.63) imply

$$\mathcal{W}_0/\zeta_0 = \frac{\mathcal{E}_m E\left[|A_m|^2\right]}{\mathcal{N}_0},$$

we verify from (II.79) that

$$\mathcal{C} \to \frac{\mathcal{E}_m E\left[|A_m|^2\right]}{\mathcal{N}_0}, \tag{II.80}$$

which we emphasize is independent of m by our power control assumption. Finally, we note that (II.80) is, of course, the capacity of the infinite-bandwidth Gaussian channel.

II.5.3 Exploiting Additional Processing Gain

For reverse link communication, co-channel interference is such that even at high SNR, the SNR γ_0 of the composite quasi-Gaussian channel for each user is low. In particular, using (II.71) in (II.65) we see that regardless of the available bandwidth or power we have

$$0 < \gamma_0 < \frac{M}{M-1}$$

for $M \geq 2$. This means that in order to achieve a throughput per user anywhere near that predicted by the capacity calculations in Section II.5.2, an enormous amount of coding is required. Conversely, without the use of coding, bit error rate performance on the reverse link will be invariably poor.

As an alternative to coding, one can consider exploiting simple spread-spectrum processing gain to raise γ_0 to a level sufficient for acceptable bit error rate performance. Although, as we shall see, direct coding is always preferable in terms of efficiency, using simple processing gain is appealing in terms of its substantial ease of implementation and reduced

computational complexity.

Augmenting our M-user system model to incorporate such processing gain is straightforward. In essence, we expand the bandwidth per user while fixing the symbol rate by replacing the up- and down-sampling rates in Figs. II.1 and II.3 with an integer L satisfying $L > M$. The resulting bandwidth expansion factor or processing gain is then

$$\rho = L/M. \tag{II.81}$$

With this change, the SNR γ_m of the composite channel becomes

$$\frac{\gamma_m}{L} = \frac{1}{\beta_m} - 1,$$

where

$$\beta_m = E\left[\frac{1 + \frac{1}{L}\sum\limits_{\substack{k=1 \\ k\neq m}}^{M} \alpha_k}{1 + \frac{1}{L}\sum\limits_{k=1}^{M} \alpha_k}\right] \tag{II.82}$$

and with α_k as in (II.60). Again, using Lemma 2 with $v_k = \alpha_k/L$ we can express (II.82) in closed form as

$$\beta_0 = \frac{M-1}{M} + \frac{(L\zeta_0)^M}{M!}\left[(-1)^{M+1}e^{L\zeta_0}E_1(L\zeta_0) + \sum_{k=0}^{M-2}(-1)^{M-k}\frac{k!}{(L\zeta_0)^{k+1}}\right]. \tag{II.83}$$

In the remainder of this section, we focus on the large number of user ($M \to \infty$) scenario. In this case, again using the law of large numbers, we get

$$\gamma_0 \sim \frac{1}{\zeta_0 + 1/\rho}, \tag{II.84}$$

where ρ is as given by (II.81). At high SNR (*i.e.*, when the receiver noise is negligible), (II.84) further simplifies to

$$\gamma_0 \sim \rho.$$

The use of processing gain permits a tradeoff between bit error rate and bandwidth. In particular, from (II.84) we see that larger processing gains invariably give rise to improved bit error rate performance. However, this improvement is obtained at the expense of bandwidth. From an information theoretic point of view, this particular tradeoff is not efficient. Too see this, note that if we apply coding on top of this new system that exploits processing gain, the apparent capacity per user per unit bandwidth is

$$\frac{\mathcal{C}}{\mathcal{W}_0\rho} = \frac{1}{\rho}\log(1+\gamma_0) = \frac{1}{\rho}\log\left(1 + \frac{1}{\zeta_0 + 1/\rho}\right) \tag{II.85}$$

where the last equality follows from (II.84). In Fig. II.8, we use (II.85) to plot capacity per user per unit bandwidth as a function of the processing gain ρ in the large number of users

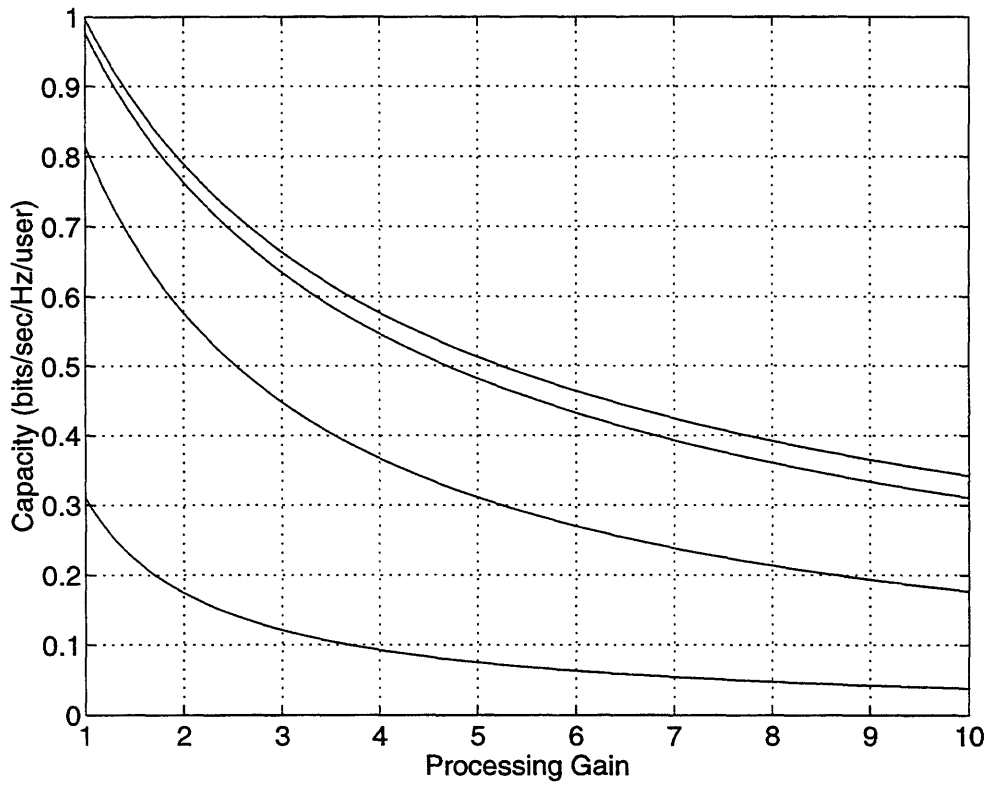

Figure II.8: *Capacity per user per unit bandwidth as a function of processing gain ρ, where the number of users satisfies $M \to \infty$. The successively higher curves correspond to SNRs of -5, 5, 15, and 25 dB.*

limit $M \to \infty$. We note that the effective capacity achievable with additional coding falls monotonically with ρ, and that the case $\rho = 1$ corresponds to our original system, *i.e.*, the system without processing gain. This is because the bandwidth expansion incurred by using a larger processing gain ρ more than offsets the increase in the SNR per symbol achieved. In fact, it is straightforward to show from (II.85) that $\mathcal{C} \to 0$ as $\rho \to \infty$.

Despite the inherent bandwidth inefficiency, exploiting processing gain is highly practical technique and enjoys widespread use. Let us consider, for example, the bit error rate performance of uncoded QPSK (quadrature phase-shift keying) using spread-signature CDMA with M users and processing gain $\rho = L/M$, some integer L. In this case, again assuming the use of power control, the bit error probability is given by

$$\mathcal{P} = \mathcal{Q}\left(\sqrt{\gamma_0}\right) \tag{II.86}$$

where

$$\mathcal{Q}(\nu) = \frac{1}{\sqrt{2\pi}} \int_{\nu}^{\infty} e^{-t^2/2}\, dt,$$

and where γ_0 is given by (II.5.3) with (II.83), or, in the case of large numbers of users, (II.84).

In Fig. II.9 we plot bit error probability as a function SNR per bit for several processing gains in the large number of user scenario, and include comparisons to conventional CDMA. In both the spread-signature and conventional CDMA systems, no channel coding is used. From this plot, it is apparent that there is an enormous advantage in using spread-signature CDMA over conventional CDMA in such uncoded systems. This is due to the fact that spread-signature CDMA is much more effective than conventional CDMA at mitigating the effects of fading even without additional coding. In particular, at high SNR and for large numbers of users, the bit error probability of spread-signature CDMA saturates at

$$\mathcal{P} \sim \mathcal{Q}(\sqrt{\rho}), \tag{II.87}$$

while for conventional CDMA the bit error probability saturates at

$$\mathcal{P}_0 \sim \frac{1}{2}\left(1 - \frac{1}{\sqrt{2/\rho + 1}}\right). \tag{II.88}$$

Finally, in Fig. II.10 we plot bit error probability as a function of processing gain for several SNR values, again in the large number of users scenario. For comparison, we also plot the performance of conventional CDMA, using (II.88).

II.6 Summary

Spread-signature CDMA as developed in this part of the report constitutes a potentially attractive alternative to conventional CDMA for general multiuser communication in fading environments. Indeed, the performance results suggest that by effectively combining modulation and precoding, such systems appear to offer significantly better performance.

Nevertheless numerous issues remain to be explored. In traditional CDMA systems, coding is used to combat the effects of fading, co-channel interference, and receiver noise. However, in spread-signature CDMA systems, the effects of fading are mitigated by the precoding implicit in the modulation, leaving coding to handle only the remaining interference and noise effects. This would appear to be a favorable computational tradeoff, since in general demodulation is computationally much cheaper than decoding. However, further simulations are required to verify these computational advantages. In addition, while we have restricted our attention to single-user detector receivers, the possibility of developing viable joint detector receivers is also worth pursuing.

Other issues, both technical and practical, also warrant further investigation. Among the technical issues, an obvious question that arises concerns the extent to which the capacity expressions developed in this report can be interpreted in a strict Shannon sense. Some of the more important practical issues which remain to be explored include receiver synchronization and peak-to-average transmitter power requirements, and equalizer sensitivity characteristics.

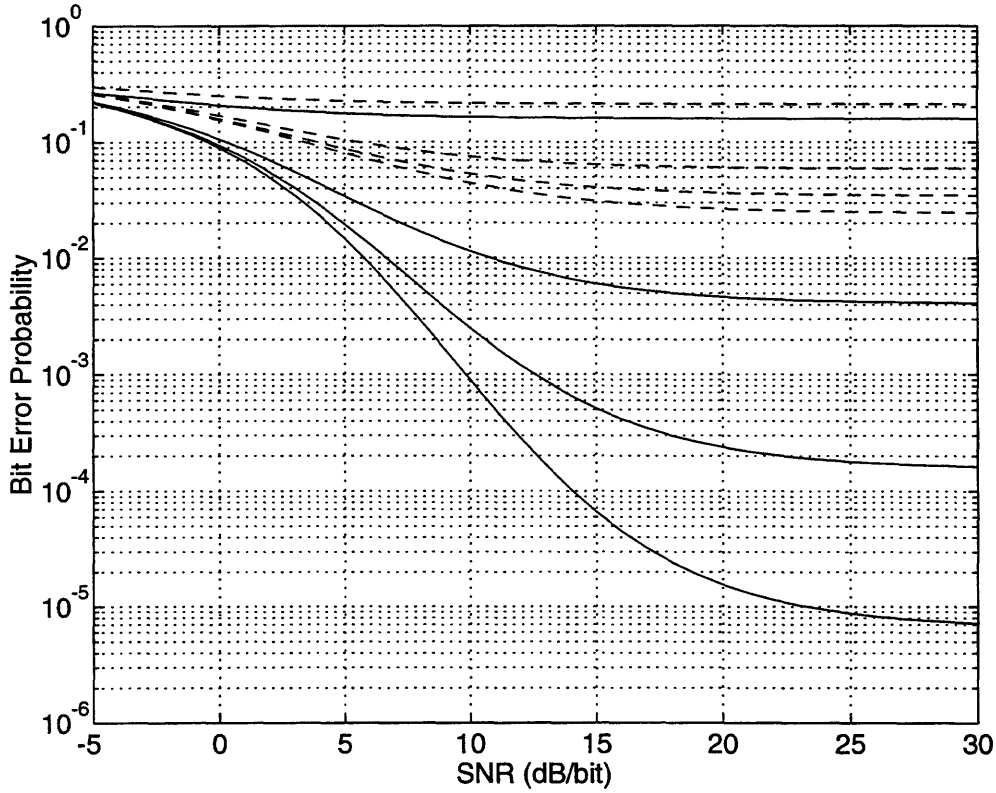

Figure II.9: *Bit error probability as a function of SNR per bit for uncoded QPSK on reverse link with $M \to \infty$ users. The successively lower solid curves correspond to the performance of spread-signature CDMA with processing gains of $\rho = 1, 7, 13, 19$. For comparison, the successively lower dashed curves correspond to the performance of conventional CDMA with the same series of processing gains. For these comparisons, no coding is used in either system.*

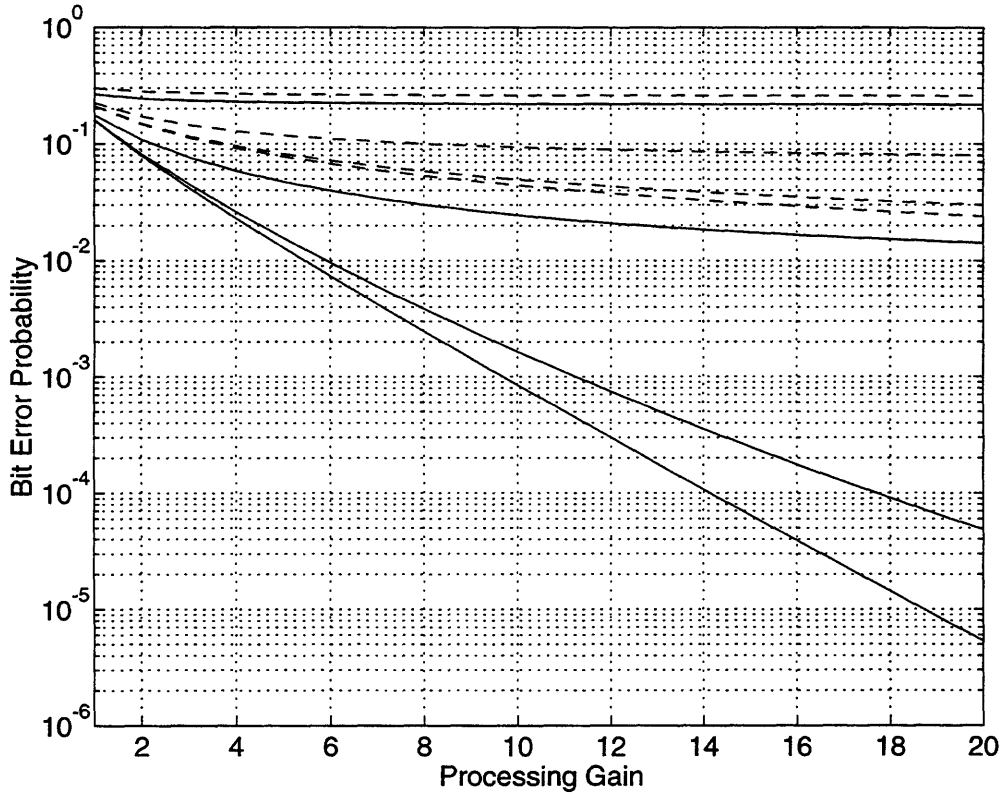

Figure II.10: *Bit error probability as a function of processing gain for uncoded QPSK on reverse link with $M \to \infty$ users. The successively lower solid curves correspond to the performance of spread-signature CDMA with SNRs of -5, 5, 15, and 25 dB/bit. For comparison, the successively lower dashed curves correspond to the performance of conventional CDMA with the same series of SNRs. For these comparisons, no coding is used in either system.*

Part III

Appendices

III.A Proof of Theorem 1

As an intermediate step, we obtain results concerning the following related system. Let $\mathcal{S}\{\cdot\}$ denote a linear system which is the cascade of an LTI system whose unit-sample response $g_1[n]$, followed by a linear system whose response at time n to an unit-sample at time $n-k$ is $f[n;k]$, followed by another LTI system whose unit sample response is $g_2[n]$. Hence,

$$q[n] = \mathcal{S}\{p[n]\} = \sum_i g_2[i] \sum_k f_k[n-i] \sum_l g_1[l]\, p[n-i-k-l] \tag{III.1}$$

Furthermore, let $u[n;k]$ denote the kernel of the overall linear system, *i.e.*, its response at time n to a unit-sample at time $n-k$.

We begin with a useful lemma regarding such systems.

Lemma 3 *Let $g_1[n]$ and $g_2[n]$ be lossless, and let $f[n;k]$ be the kernel of an admissibly ergodic system. Then as*

$$\mathcal{D}_2 = \left(\sum_i g_2^4[i]\right)^{-1} \to \infty, \tag{III.2}$$

the kernel $u[n;k]$ defined above obeys

$$u[n;k] \xrightarrow{\text{m.s.}} \mu\,(g_1[k] * g_2[k]) \triangleq u[k] \tag{III.3}$$

and

$$\sum_k \tilde{u}[n;n-k]\,\tilde{u}^*[m;m-k] \xrightarrow{\text{m.s.}} \sigma^2\delta[n-m] \tag{III.4}$$

where

$$\tilde{u}[n;k] = u[n;k] - u[k].$$

Proof:
From (III.1) we get

$$u[n;k] = \sum_i g_2[i] \sum_l f[n-i;l]\, g_1[k-i-l]. \tag{III.5}$$

Then

$$E\,[u[n;k]] = \mu \sum_i g_2[i]\, g_1[k-i] = \mu_c \cdot g_1[k] * g_2[k]$$

and

$$\tilde{u}[n;k] = \sum_i g_2[i] \sum_l \tilde{f}[n-i;l]\, g_1[k-i-l]$$

where, consistent with (I.14),

$$\tilde{f}[n;k] = f[n;k] - \mu\, \delta[k].$$

Hence,

$$E\left[|\tilde{u}[n;k]|^2\right] = \sum_{i,i'} \sum_l g_2[i]\, g_2[i']\, R[i'-i;l]\, g_1[k-l-i]\, g_1[k-l-i'] \tag{III.6}$$

where $R[m;k]$ is as defined in (I.17b). Applying, in order, the triangle inequality and the Cauchy inequality, we are able to bound (III.6) by

$$E\left[|\tilde{u}[n,k]|^2\right] \leq \varphi(g_1)\, \varphi(g_2) \tag{III.7}$$

where

$$\varphi^2(g) = \sum_{i,i',l} |R[i'-i;l]|\, g^2[i]\, g^2[i'] \leq S_R$$

provided

$$\sum_n g^2[n] \leq 1.$$

Applying the Cauchy inequality again to $\varphi^2(g_2)$, however, gives, after some simplification and using (III.2),

$$\varphi^2(g_2) \leq S_R/\mathcal{D}_2. \tag{III.8}$$

Hence, (III.8) and, in turn, (III.6) tend to zero as $\mathcal{D}_2 \to \infty$, which verifies (III.3).

To show (III.4), we begin by noting that since $g_1[n]$ is lossless, we get, using (I.15),

$$\rho[n,m] \triangleq \sum_k \tilde{u}[n;n-k]\, \tilde{u}^*[m;m-k] = \sum_{i,l} g_2[n-i]\, g_2[m-i+l]\, d[i;l].$$

Then, since by (I.17b)

$$E\,[d[n;k]] = \sigma^2\, \delta[k],$$

we get, using (I.25),

$$E\,[\rho[n,m]] = \sigma^2\, \delta[n-m].$$

Next, we write, using (I.16),

$$\tilde{\rho}[n,m] \triangleq \rho[n,m] - \sigma^2 \delta[n-m] = \sum_{i,l} g_2[n-i]\, g_2[m-i+l]\, \tilde{d}[i;l]$$

and, using (I.17c)

$$E\left[|\tilde{\rho}[n,m]|^2\right] = \sum_{i,i',l,l'} g_2[n-i]\, g_2[m-i+l]\, g_2[n-i']\, g_2[m-i'+l']\, T[i-i';l,l']. \quad \text{(III.9)}$$

However, applying the triangle and Cauchy inequalities, in order, and noting

$$T[m;k,l] = T^*[-m;l,k]$$

we can bound (III.9) by

$$E\left[|\tilde{\rho}[n,m]|^2\right] \leq \sum_{i,i',l,l'} g_2^2[n-i]\, g_2^2[m-i+l]\, \left|T[i-i';l,l']\right|. \quad \text{(III.10)}$$

Applying the triangle and Cauchy inequalities, in order, again, to the right side of (III.10), and changing variables, we get

$$E\left[|\tilde{\rho}[n,m]|^2\right] \leq \sum_{i,i',l,l'} g_2^4[i]\, \left|T[i';l,l']\right| = S_T/\mathcal{D}_2. \quad \text{(III.11)}$$

which approaches zero as $\mathcal{D}_2 \to \infty$. ■

Using Lemma 3, we obtain the following theorem:

Theorem 4 *Let $g_1[n]$ and $g_2[n]$ be lossless, and let $f[n;k]$ be an admissibly ergodic system kernel. Further, and suppose $p[n]$ is a wide-sense stationary, white random process with mean zero and variance σ^2, and that $p[n]$ and the channel kernel $f[n;k]$ are statistically independent. Then, as $\mathcal{D}_2 \to \infty$, $q[n]$ as defined by (III.1) satisfies, with $u[n]$ as defined in (III.3),*

$$q[n] \xrightarrow{\text{m.s.}} u[n] * p[n] + z[n], \quad \text{(III.12)}$$

where $z[n]$ is a marginally Gaussian wide-sense stationary, white random process with mean zero and variance $\sigma^2\sigma^2$, and where $z[n]$ is uncorrelated with $p[n]$.

Proof:
By superposition,

$$q[n] = \sum_k u[n;k]\, p[n-k];$$

hence,

$$z[n] = q[n] - u[n] * p[n] = \sum_k \tilde{u}[n;k]\, p[n-k]. \quad \text{(III.13)}$$

From (III.13) we get immediately, since $p[n]$ is zero-mean,

$$E_p\left[z[n]\right] = 0,$$

where we use $E_p[\cdot]$ to denote expectation with respect to $p[n]$ given a fixed but arbitrary realization of the kernel $f[n;k]$.

In addition, from (III.13) we get

$$E_p\left[z[n]\,p^*[m]\right] = \sum_k \tilde{u}[n;k]\,E_p\left[p[n-k]\,p^*[m]\right] = \sigma^2\tilde{u}[n;n-m]. \tag{III.14}$$

Hence, since (III.3) in Lemma 3 implies

$$\tilde{u}[n;k] \xrightarrow{\text{m.s.}} 0,$$

we get, from (III.14),

$$E_p\left[z[n]\,p^*[m]\right] \xrightarrow{\text{m.s.}} 0 \quad \text{as } \mathcal{D}_2 \to \infty.$$

Finally, using (III.13) we also obtain

$$\begin{aligned} E_p\left[z[n]\,z^*[m]\right] &= \sum_{k,l} \tilde{u}[n;k]\,\tilde{u}^*[m;l]E_p\left[p[n-k]\,p^*[m-l]\right] \\ &= \sigma^2 \sum_k \tilde{u}[n;n-k]\,\tilde{u}^*[m;m-k]. \end{aligned} \tag{III.15}$$

Applying (III.4) in Lemma 3 to (III.15), we see immediately

$$E_p\left[z[n]\,z^*[m]\right] \xrightarrow{\text{m.s.}} \sigma^2\sigma^2\delta[n-m] \quad \text{as } \mathcal{D}_2 \to \infty.$$

Finally, to show that $z[n]$ is marginally Gaussian requires a straightforward Central Limit Theorem argument. ■

The following pair of corollaries lead directly to a proof of our main theorem.

Corollary 1 *Suppose $g_1[n] = g_2[-n]$ in Theorem 4. Then as $\mathcal{D}_2 \to \infty$,*

$$q[n] \xrightarrow{\text{m.s.}} \mu\,p[n] + z[n]. \tag{III.16}$$

Proof:
It suffices to note that, since $g_2[n]$ is lossless

$$g_1[n] * g_2[n] = g_2[n] * g_2[-n] = \delta[n].$$

■

Corollary 2 *Suppose $g_1[n] = \delta[n]$. Then $q[n]$ is white and has variance*

$$\text{var}_{\text{p}}\,q[n] = E_p\left[|q[n]|^2\right] = \sigma^2|\mu|^2 + \sigma^2\sigma^2 = \sigma^2 E\left[|F(\omega;n)|^2\right]. \tag{III.17}$$

Proof:
Since $p[n]$ and $z[n]$ are uncorrelated in Theorem 4,

$$\text{var}_{\text{p}}\,q[n] = \text{var}_{\text{p}}\,\left(\mu g_2[n] * p[n]\right) + \text{var}_{\text{p}}\,z[n]. \tag{III.18}$$

Furthermore, since $g_2[n]$ is lossless, $p[n]$ and $p[n] * g_2[n]$ have the same spectrum and thus

$$\mathrm{var_p}\ (\mu g_2[n] * p[n]) = |\mu|^2 \sigma^2.$$

Applying (I.25) and (I.19) we then verify (III.17). ■

Finally, to establish Theorem 1 we need only recognize that $\hat{x}[n]$ can be divided into two uncorrelated components:

$$\hat{x}[n] = \hat{x}_1[n] + \hat{x}_2[n],$$

where $\hat{x}_1[n]$ is the component due to $x[n]$ and where $\hat{x}_2[n]$ is due to $w[n]$. Using Theorem 4 and Corollary 1 with $p[n] = x[n]$, $q[n] = \hat{x}_1[n]$, and $f[n;k] = c[n;k]$, we see

$$\hat{x}_1[n] \xrightarrow{\text{m.s.}} \mu_c\, x[n] + z[n]$$

where the white noise $z[n]$ has variance $\mathcal{E}_s \sigma_c^2$. Similarly, using Theorem 4 and Corollary 2 with $p[n] = w[n]$, $q[n] = \hat{x}_2[n]$, and $f[n;k] = b[n;k]$ we get that

$$\mathrm{var}\, \hat{x}_2[n] = \mathcal{N}_0 \mathcal{W}_0 E\left[|B(\omega;n]|^2\right].$$

■

III.B Linear Randomly Time-Varying Systems

We adopt the following notation for linear randomly time-varying systems corresponding to wide-sense stationary uncorrelated scattering. We begin by using $f[n;k]$ to denote the kernel of a discrete-time linear system, corresponding to the response of the system at time n to a unit sample at time $n-k$. Hence, the response of the system to an input $x[n]$ is

$$y[n] = \sum_k f[n;k]\, x[n-k].$$

The time-variant system frequency response associated with this system is denoted by

$$F(\omega;n] = \sum_k f[n;k]\, e^{-j\omega k}, \tag{III.19}$$

and represents the response of the system to complex exponential $e^{j\omega n}$. For stationary systems, we define the system correlation function by

$$R[m;k] = E\left[\tilde{f}[n;k]\, \tilde{f}^*[n-m;k]\right].$$

where

$$\tilde{f}[n;k] = f[n;k] - E\left[f[n;k]\right],$$

and the system scattering function by

$$S(\lambda;k] = \sum_m R[m;k]\, e^{-j\lambda m}.$$

When the system is characterized by uncorrelated scattering we have both

$$E\left[f[n;k]\right] = E\left[f[n;0]\right]\,\delta[k]$$

and

$$E\left[\tilde{f}[n;k]\,\tilde{f}^{*}[n-m;l]\right] = R[m;k]\,\delta[k-l].$$

This makes $D(\omega;n]$ defined in (III.19) wide-sense stationary in both ω and n, a property we exploit extensively.

Another useful characterization of such systems is in terms of the associated spaced-frequency spaced-time correlation function, which is given by

$$\Psi(\omega;m] = \sum_{k} R[m;k]\,e^{-j\omega k} = E\left[\tilde{F}(\theta;n]\,\tilde{F}^{*}(\theta-\omega;n-m]\right]$$

where

$$\tilde{F}(\omega;n] = F(\omega;n] - E\left[F(\omega;n]\right].$$

In turn, we define the system Doppler power spectrum by

$$\Upsilon(\lambda) = \sum_{m} \Psi(0;m]\,e^{j\lambda m}.$$

Finally, the multipath intensity profile or delay power spectrum of the system is

$$\Pi[k] = R[0;k] = \operatorname{var} f[n;k],$$

so the total power is

$$\operatorname{var} F(\omega;n] = \Psi(0;0] = \sum_{k} \Pi[k].$$

III.C Maximally Spread Signature Sequences

Coefficients are first converted to a binary sequence, with $1/\sqrt{N}$ represented by '1' and $-1/\sqrt{N}$ represented by '0', then replaced with the hexidecimal equivalent.

M	N	$\mathbf{h}[n]$
2	4	E
		D
4	4	F
		A
		C
		9
2	8	ED
		E2
8	8	FF
		AA
		CC
		99
		F0
		A5
		C3
		96
2	16	EDE2
		ED1D
4	16	FAC9
		F5C6
		FA36
		F539
2	32	EDE2ED1D
		EDE212E2
2	64	EDE2ED1DEDE212E2
		EDE2ED1D121DED1D
4	64	FAC9F5C6FA36F539
		FAC90A39FA360AC6
		FAC9F5C605C90AC6
		FAC90A3905C9F539
8	64	FFAACC99F0A5C396
		FF55CC66F05AC369
		FFAA3366F0A53C69
		FF553399F05A3C96
		FFAACC990F5A3C69
		FF55CC660FA53C96
		FFAA33660F5AC396
		FF5533990FA5C369
2	128	EDE2ED1DEDE212E2EDE2ED1D121DED1D
		EDE2ED1DEDE212E2121D12E2EDE212E2
2	256	EDE2ED1DEDE212E2EDE2ED1D121DED1DEDE2ED1DEDE212E2121D12E2EDE212E2
		EDE2ED1DEDE212E2EDE2ED1D121DED1D121D12E2121DED1DEDE2ED1D121DED1D
4	256	FAC9F5C6FA36F539FAC90A39FA360AC6FAC9F5C605C90AC6FAC90A3905C9F539
		FAC9F5C6FA36F5390536F5C605C9F539FAC9F5C605C90AC60536F5C6FA360AC6
		FAC9F5C6FA36F539FAC90A39FA360AC605360A39FA36F5390536F5C6FA360AC6
		FAC9F5C6FA36F5390536F5C605C9F53905360A39FA36F539FAC90A3905C9F539

III.D Proofs of Theorems 2 and 3

It is convenient to develop some intermediate results for a family of related systems. Let $\mathcal{S}_{ij}\{\cdot\}$ denote a linear system which is the cascade of a rate-M upsampler, an LTI system whose unit-sample response is $h_i[n]$, a linear time varying system whose kernel is $f_{ij}[n;k]$, another LTI system with unit-sample response $h_j[-n]$, and finally a rate-M downsampler. Hence

$$q[n] = \mathcal{S}_{ij}\{p[n]\} = \sum_{m,l,k} f_{ij}[m;l]\, h_j[m-nM]\, h_i[m-l-kM]\, p[k], \tag{III.20}$$

and it is straightforward to show that the kernel of this system is

$$u_{ij}[n;k] = \sum_{m,l} f_{ij}[nM+m; kM+l]\, h_j[m]\, h_i[m-l]. \tag{III.21}$$

We begin with the following lemma.

Lemma 4 *Let $h_i[n]$ and $h_j[n]$ be chosen from an set of M orthogonal signatures, and let $f_{ij}[n;k]$ for $j = 1, 2, \ldots, M$ be an admissibly ergodic family of kernels in the sense of Definition 2. Then, with $\mathcal{D}_h$ and χ_h as defined in (II.21) and (II.29), respectively, as $\mathcal{D}_h \to \infty$ and $\chi_h \to \infty$, the kernel (III.21) obeys*

$$u_{ij}[n;k] \xrightarrow{\text{m.s.}} E\,[F_{ii}]\ \delta[k]\,\delta[i-j] \triangleq u_{ij}[k] \tag{III.22}$$

and

$$\sum_k \tilde{u}_{ij}[n;n-k]\, \tilde{u}^*_{ij'}[m;m-k] \xrightarrow{\text{m.s.}} \frac{1}{M}\text{var}\,[F_{ij}]\ \delta[n-m]\,\delta[j-j'] \tag{III.23}$$

where

$$\tilde{u}_{ij}[n;k] = u_{ij}[n;k] - u_{ij}[k].$$

Proof:

Using (II.44a) with (III.21), we obtain

$$\begin{aligned} E\,[u_{ij}[n;k]] &= E\,[F_{ij}] \sum_l h_j[l] h_i[l+kM] \\ &= E\,[F_{ii}]\ \delta[i-j]\,\delta[k] \end{aligned} \tag{III.24}$$

and

$$\tilde{u}_{ij}[n;k] = \sum_{m,l} \tilde{f}_{ij}[nM+m; kM+l]\, h_j[m]\, h_i[m-l] \tag{III.25}$$

where $\tilde{f}_{ij}[n;k]$ is as defined in (II.41).

From (III.25) we get

$$E\,[|\tilde{u}_{ij}[n;k]|^2] = \sum_{m,m',l} R^{ij'}_{ij}[m-m'; kM-l]\, h_j[m]\, h_j[m']\, h_i[l+m]\, h_i[l+m'], \tag{III.26}$$

where $R_{ij}^{ij}[n;k]$ is as defined in (II.44b). Applying, in order, the triangle inequality and the Cauchy inequality, (III.26) can be bounded by

$$E\left[|\tilde{u}_{ij}[n;k]|^2\right] \leq \varphi(h_i)\,\varphi(h_j) \tag{III.27}$$

where

$$\varphi^2(g) = \sum_{m,m',l} |R_{ij}^{ij}[m-m';kM-l]|\, g^2[m]\, g^2[m']. \tag{III.28}$$

Applying the Cauchy inequality again to $\varphi^2(g)$, however, gives, after some simplification, and using (II.44d),

$$\varphi^2(g) \leq S_{R_{ij}^{ij}}/\mathcal{D}_g$$

where

$$\mathcal{D}_g = \left(\sum_n g^4[n]\right)^{-1}.$$

Hence,

$$E\left[|\tilde{u}_{ij}[n;k]|^2\right] \leq \frac{S_{R_{ij}^{ij}}}{\sqrt{\mathcal{D}_{h_i}\,\mathcal{D}_{h_j}}} \tag{III.29}$$

which tends to zero as $\mathcal{D}_h \to \infty$. Collectively, (III.24) and (III.29) establish (III.22).

To show (III.23), we begin by noting that

$$\begin{aligned}\rho_{ij}^{ij'}[n,m] &\triangleq \sum_k \tilde{u}_{ij}[n;n-k]\,\tilde{u}_{ij'}^{*}[m;m-k] \\ &= \sum_{s,s'}\sum_{t,t'} \tilde{f}_{ij}[nM+s;t]\,\tilde{f}_{ij'}^{*}[mM+s';t']\,h_j[s]\,h_j'[s']\,\Theta_{h_i}[nM+s-t,mM+s'-t']\end{aligned}$$

where $\Theta_{h_i}[n,m]$ is as defined in (II.25).

Using (II.44b), we obtain

$$E\left[\rho_{ij}^{ij'}[n,m]\right] = \sum_{s,s',t} R_{ij}^{ij'}[(n-m)M+s-s';t]\,h_j[s]\,h_{j'}[s']\,\Theta_{h_i}[nM+s-t,mM+s'-t]$$

which, with

$$\check{\rho}_{ij}^{ij'}[n,m] \triangleq \sum_{s,s',t} R_{ij}^{ij'}[(n-m)M+s-s';t]\,h_j[s]\,h_{j'}[s']\,\tilde{\Theta}_{h_i}[nM+s-t,mM+s'-t] \tag{III.30}$$

and using (II.27), can be rewritten as

$$\begin{aligned}E\left[\rho_{ij}^{ij'}[n,m]\right] &= \check{\rho}_{ij}^{ij'}[n,m] + \frac{1}{M}\sum_t R_{ij}^{ij'}[0;t]\sum_s h_j[s]\,h_{j'}[s+(n-m)M] \\ &= \check{\rho}_{ij}^{ij'}[n,m] + \frac{1}{M}\mathrm{var}\,[F_{ij}]\,\delta[j-j']\,\delta[n-m].\end{aligned} \tag{III.31}$$

Now applying the triangle inequality and the Cauchy inequality to (III.31), we obtain the bound

$$\left|\check{\rho}_{ij}^{ij'}[n,m]\right| \leq \xi_1\xi_2 \tag{III.32}$$

where

$$\xi_1^2 = \sum_{s,s',t} \left| R_{ij}^{ij'}[(n-m)M + s - s'; t]\, h_j[s]\, h_{j'}[s'] \right| \tag{III.33}$$

and

$$\xi_2^2 = \sum_{s,s',t} \left| R_{ij}^{ij'}[(n-m)M + s - s'; t]\, h_j[s]\, h_{j'}[s'] \right| \tilde{\Theta}_{h_i}^2[nM + s - t, mM + s' - t]. \tag{III.34}$$

Applying the Cauchy inequality to (III.34) yields

$$\xi_2^2 \leq \xi_1 \xi_3 \tag{III.35}$$

where

$$\xi_3^2 = \sum_{s,s',t} \left| R_{ij}^{ij'}[(n-m)M + s - s'; t]\, h_j[s]\, h_{j'}[s'] \right| \tilde{\Theta}_{h_i}^4[nM + s - t, mM + s' - t]. \tag{III.36}$$

Similarly, applying the Cauchy inequality to (III.33) yields

$$\begin{aligned} \xi_1^4 &\leq \left(\sum_{s,s',t} \left| R_{ij}^{ij'}[(n-m)M + s - s'; t] \right| h_j^2[s] \right) \\ &\quad \cdot \left(\sum_{s,s',t} \left| R_{ij}^{ij'}[(n-m)M + s - s'; t] \right| h_{j'}^2[s'] \right) \\ &= S_{R_{ij}^{ij'}}^2 \end{aligned} \tag{III.37}$$

Similarly, applying the Cauchy inequality to (III.36) yields

$$\begin{aligned} \xi_3^4 &\leq \left(\sum_{s,s',t} \left| R_{ij}^{ij'}[(n-m)M + s - s'; t] \right| h_j^2[s]\, \tilde{\Theta}_{h_i}^4[nM + s - t, mM + s' - t] \right) \cdot \\ &\quad \cdot \left(\sum_{s,s',t} \left| R_{ij}^{ij'}[(n-m)M + s - s'; t] \right| h_{j'}^2[s']\, \tilde{\Theta}_{h_i}^4[nM + s - t, mM + s' - t] \right) \cdot \\ &\leq \frac{S_{R_{ij}^{ij'}}^2}{\chi_{h_i}^2} \end{aligned} \tag{III.38}$$

where the last inequality in (III.38) results from using, in order, the simple bound

$$\left| R_{ij}^{ij'}[n; k] \right| \leq S_{R_{ij}^{ij'}}^2 .$$

and (II.30).

Using (III.37), (III.38) and (III.35) with (III.39) we get

$$\left| \check{\rho}_{ij}^{ij'}[n, m] \right| \leq \frac{S_{R_{ij}^{ij'}}^{5/4}}{\sqrt{\chi_{h_i}}} \tag{III.39}$$

which tends to zero as $\chi_h \to \infty$.

Next, we define

$$\tilde{\rho}_{ij}^{ij'}[n,m] = \rho_{ij}^{ij'}[n,m] - E\left[\rho_{ij}^{ij'}[n,m]\right]$$

and note

$$\tilde{\rho}_{ij}^{ij'}[n,m] = \sum_{s,s'}\sum_{k,k'} \tilde{d}_{ij}^{ij'}[s,s';k,k']\,\Theta_{h_i}[s-k;s'-k']\,h_j[s-nM]\,h_{j'}[s'-mM] \tag{III.40}$$

where $\tilde{d}_{ij}^{ij'}[s,s';t,t']$ is as defined in (II.43) and (II.42).

In turn, using (II.44c) with (III.40), we get

$$\begin{aligned} E\left[\left|\tilde{\rho}_{ij}^{ij'}[n,m]\right|^2\right] = \sum_{\substack{s,s'\\k,k'}}\sum_{\substack{t,t'\\l,l'}} & T_{ij}^{ij'}[s-s',t-t',s-t;k,k',l,l'] \\ & \Theta_{h_i}[s-k;s'-k']\,\Theta_{h_i}[t-l;t'-l'] \\ & h_j[s-nM]\,h_{j'}[s'-mM]\,h_j[t-nM]\,h_{j'}[t'-mM] \end{aligned} \tag{III.41}$$

Now, from a simple application of the Cauchy inequality to (II.25) we obtain

$$|\Theta_{h_i}[n,m]| \le 1. \tag{III.42}$$

Applying, in turn, the triangle inequality, the bound (III.42), and the Cauchy inequality to (III.41) we obtain

$$\begin{aligned} E\left[\left|\tilde{\rho}_{ij}^{ij'}[n,m]\right|^2\right]^2 \le & \left(\sum_{\substack{s,s'\\k,k'}}\sum_{\substack{t,t'\\l,l'}}\left|T_{ij}^{ij'}[s-s',t-t',s-t;k,k',l,l']\right| h_j^2[s-nM]\,h_{j'}^2[s'-mM]\right) \\ & \cdot\left(\sum_{\substack{s,s'\\k,k'}}\sum_{\substack{t,t'\\l,l'}}\left|T_{ij}^{ij'}[s-s',t-t',s-t;k,k',l,l']\right| h_j^2[t-nM]\,h_{j'}^2[t'-mM]\right) \end{aligned} \tag{III.43}$$

Applying the Cauchy inequality once again to the right-hand side terms of (III.43) yields

$$\begin{aligned} E\left[\left|\tilde{\rho}_{ij}^{ij'}[n,m]\right|^2\right]^4 \le & \\ & \left(\sum_{\substack{s,s'\\k,k'}}\sum_{\substack{t,t'\\l,l'}}\left|T_{ij}^{ij'}[s-s',t-t',s-t;k,k',l,l']\right| h_j^4[s-nM]\right) \\ & \cdot\left(\sum_{\substack{s,s'\\k,k'}}\sum_{\substack{t,t'\\l,l'}}\left|T_{ij}^{ij'}[s-s',t-t',s-t;k,k',l,l']\right| h_{j'}^4[s'-mM]\right) \\ & \cdot\left(\sum_{\substack{s,s'\\k,k'}}\sum_{\substack{t,t'\\l,l'}}\left|T_{ij}^{ij'}[s-s',t-t',s-t;k,k',l,l']\right| h_j^4[t-nM]\right) \end{aligned} \tag{III.44}$$

$$\cdot \left(\sum_{\substack{s,s' \\ k,k'}} \sum_{\substack{t,t' \\ l,l'}} \left| T_{ij}^{ij'}[s-s', t-t', s-t; k, k', l, l'] \right| \, h_{j'}^4[t' - mM] \right)$$

$$= \frac{S_{T_{ij}^{ij'}}^4}{\mathcal{D}_{h_j}^2 \mathcal{D}_{h_{j'}}^2} \tag{III.45}$$

which tends to zero as $\mathcal{D}_h \to \infty$. Collectively, (III.31), (III.39), and (III.45) establish (III.23).
■

Proposition 1 *Suppose that the input to the system defined by (III.21) is a zero-mean, white Gaussian sequence $p_i[n]$ with variance σ_i^2, and let the corresponding output sequence be $q_{ij}[n]$. Moreover, assume that for different values of i the sequences $p_i[n]$ are mutually independent. Then given the same hypotheses of Lemma 4, we have*

$$q_{ij}[n] \xrightarrow{\text{m.s.}} E[F_{ii}] \, \delta[i-j] \, p_i[n] + z_{ij}[n] \tag{III.46}$$

where the $z_{ij}[n]$ are mutually uncorrelated, zero-mean white marginally Gaussian sequences with variances $\sigma_i^2 \text{var}[F_{ij}]/M$, i.e.,

$$E[z_{ij}[n]] = 0 \tag{III.47a}$$

$$E[z_{ij}[n] \, p_{i'}^*[m]] = 0 \tag{III.47b}$$

$$E[z_{ij}[n] \, z_{i'j'}[m]] = \delta[i-i'] \, \delta[j-j'] \, \delta[n-m] \, \frac{1}{M} \sigma_i^2 \text{var}[F_{ij}]. \tag{III.47c}$$

Furthermore, we have that the sequences $q_{ij}[n]$ are zero-mean and white with variance

$$\text{var} \, q_{ij}[n] = \delta[i-j] \sigma_i^2 \, |E[F_{ii}]|^2 + \frac{1}{M} \sigma_i^2 \, \text{var}[F_{ij}] \tag{III.48}$$

and are mutually uncorrelated for different values of j.

Proof:

We begin by noting that

$$q_{ij}[n] = \sum_k u_{ij}[n;k] \, p_i[n-k]$$

can be rewritten as

$$q_{ij}[n] = E[F_{ii}] \, \delta[i-j] \, p[n] + z_{ij}[n]$$

where

$$z_{ij}[n] = \sum_k \tilde{u}_{ij}[n;k] \, p_i[n-k]. \tag{III.49}$$

From (III.49) we get immediately, since $p_i[n]$ is zero-mean, that $z_{ij}[n]$ satisfies (III.47a), *i.e.*,

$$E_p[z_{ij}[n]] = 0,$$

where we use $E_p[\cdot]$ to denote expectation with respect to $p[n]$ given fixed but arbitrary realizations of the kernels $f_{ij}[n;k]$.

In addition, from (III.49) we get

$$E_p\left[z_{ij}[n]\, p^*_{i'}[m]\right] = \sigma_i^2\, \delta[i-i']\, \tilde{u}[n; n-m]. \tag{III.50}$$

Hence, since (III.22) in Lemma 4 implies

$$\tilde{u}[n;k] \xrightarrow{\text{m.s.}} 0,$$

we get, from (III.50), the result (III.47b), *i.e.*

$$E_p\left[z_{ij}[n]\, p_{i'}[m]\right] \xrightarrow{\text{m.s.}} 0.$$

Finally, using (III.49) we also obtain

$$\begin{aligned} E_p\left[z_{ij}[n]\, z^*_{ij'}[m]\right] &= \sigma_i^2\, \delta[i-i'] \sum_{k,l} \tilde{u}_{ij}[n;k]\, \tilde{u}^*_{ij'}[m;l] E_p\left[p_i[n-k]\, p_i[m-l]\right] \\ &= \sigma_i^2\, \delta[i-i'] \sum_{k} \tilde{u}_{ij}[n; n-l]\, \tilde{u}^*_{ij'}[m; m-l]. \end{aligned} \tag{III.51}$$

Applying (III.23) in Lemma 4 to (III.51) we obtain (III.47c) immediately, *i.e.*,

$$E_p\left[z_{ij}[n]\, z^*_{ij'}[m]\right] \to \sigma_i^2\, \delta[i-i'] \frac{1}{M} \text{var}\left[F_{ij}\right]\, \delta[n-m]\, \delta[j-j'].$$

Finally, to show that $z_{ij}[n]$ is marginally Gaussian requires a straightforward Central Limit Theorem argument.

■

III.D.1 The Forward Link Theorem

Using Proposition 1, we can readily establish Theorem 2. In particular, due to linearity we can partition $\hat{x}_m[n]$ into two components: $\hat{x}^{(1)}_m[n]$, which is generated by the set of transmitted sequences $x_i[n]$, and $\hat{x}^{(2)}_m[n]$, which is generated by the background noise $w[n]$.

We first note that if in Proposition 1 we let $p_i[n] = x_i[n]$ and $f_{ij}[n;k] = c[n;k]$, then we readily obtain, using superposition, that

$$\hat{x}^{(1)}_m[n] = \sum_{i=1}^{M} q_{im}[n] \xrightarrow{\text{m.s.}} E\left[C\right] x_m[n] + v^{(1)}_m[n], \tag{III.52}$$

where

$$v^{(1)}_m[n] = \sum_{i=1}^{M} z_{im}[n].$$

Note, in addition, that due to the properties of the $z_{ij}[n]$ in Proposition 1 the $v^{(1)}_m[n]$ are mutually uncorrelated, zero-mean, white marginally-Gaussian noise sequences with variances

$$\text{var}\, v^{(1)}_m[n] = \text{var}\left[C\right] \frac{1}{M} \sum_{i=1}^{M} \mathcal{E}_i \tag{III.53}$$

Next we note that if in Proposition 1 we let $p_i[n] = \sum_k w[k]\, h_m[k - nM]$ and $f_{ij}[n;k] = b[n;k]$, then we again readily obtain that

$$\hat{x}_m^{(2)}[n] = \sum_{i=1}^{M} q_{im}[n] \xrightarrow{\text{m.s.}} v_m^{(2)}[n], \tag{III.54}$$

where the $v_m^{(2)}[n]$ are mutually uncorrelated, zero-mean, white marginally Gaussian noise sequences with variances

$$\operatorname{var} v_m^{(2)}[n] = \mathcal{N}_0 \mathcal{W}_0 |E[B]|^2 + \mathcal{N}_0 \mathcal{W}_0 \operatorname{var}[B] = \mathcal{N}_0 \mathcal{W}_0 E\left[|B|^2\right]. \tag{III.55}$$

Hence, combining (III.52) and (III.54) we obtain (II.46) where

$$v_m[n] = v_m^{(1)}[n] + v_m^{(2)}[n].$$

Furthermore, since the $x_m[n]$ and $w[n]$ are uncorrelated, we obtain (II.47) using

$$\operatorname{var} v_m[n] = \operatorname{var} v_m^{(1)}[n] + \operatorname{var} v_m^{(2)}[n]$$

with (III.53) and (III.55).

III.D.2 The Reverse Link Theorem

Using Proposition 1, we can also readily establish Theorem 3. Again, exploiting linearity we partition $\hat{x}_m[n]$ into two components: $\hat{x}_m^{(1)}[n]$, which is generated by the set of transmitted sequences $x_i[n]$, and $\hat{x}_m^{(2)}[n]$, which is generated by the background noise $w[n]$.

When in Proposition 1 we let $p_i[n] = x_i[n]$ and $f_{ij}[n;k] = c_{ij}[n;k]$, we readily obtain, using superposition, that

$$\hat{x}_m^{(1)}[n] = \sum_{i=1}^{M} q_{im}[n] \xrightarrow{\text{m.s.}} E[C_{mm}]\, x_m[n] + v_m^{(1)}[n], \tag{III.56}$$

where

$$v_m^{(1)}[n] = \sum_{i=1}^{M} z_{im}[n].$$

Note, in addition, that due to the properties of the $z_{ij}[n]$ in Proposition 1, the $v_m^{(1)}[n]$ are mutually uncorrelated, zero-mean, white marginally-Gaussian noise sequences with variances

$$\operatorname{var} v_m^{(1)}[n] = \frac{1}{M} \sum_{i=1}^{M} \mathcal{E}_i \operatorname{var}[C_{im}]. \tag{III.57}$$

Next, when in Proposition 1 we let $p_i[n] = \sum_k w[k]\, h_m[k - nM]$ and $f_{ij}[n;k] = b_j[n;k]$,

we again readily obtain that

$$\hat{x}_m^{(2)}[n] = \sum_{i=1}^{M} q_{im}[n] \xrightarrow{\text{m.s.}} v_m^{(2)}[n], \tag{III.58}$$

where the $v_m^{(2)}[n]$ are mutually uncorrelated, zero-mean, white marginally Gaussian noise sequences with variances

$$\text{var}\, v_m^{(2)}[n] = \mathcal{N}_0\mathcal{W}_0|E\left[B_m\right]|^2 + \mathcal{N}_0\mathcal{W}_0\text{var}\left[B_m\right] = \mathcal{N}_0\mathcal{W}_0 E\left[|B_m|^2\right]. \tag{III.59}$$

Hence, combining (III.56) and (III.58) we obtain (II.55 where

$$v_m[n] = v_m^{(1)}[n] + v_m^{(2)}[n].$$

Furthermore, since the $x_m[n]$ and $w[n]$ are uncorrelated, we obtain (II.56) using

$$\text{var}\, v_m[n] = \text{var}\, v_m^{(1)}[n] + \text{var}\, v_m^{(2)}[n]$$

with (III.57) and (III.59).

III.E Proof of Lemma 1

First, note we may rewrite (II.58) in the form

$$\gamma_m(B) = \frac{\mathcal{E}_m\left|E\left[A_m\, B\right]\right|^2}{E\left[|\xi B|^2\right] - \frac{1}{M}\sum_k \mathcal{E}_k\left|E\left[A_k\, B\right]\right|^2} \tag{III.60}$$

where

$$\xi = \sqrt{\mathcal{N}_0\mathcal{W}_0 + \frac{1}{M}\sum_k \mathcal{E}_k|A_k|^2}. \tag{III.61}$$

Using the invertible change of variables

$$\tilde{B} = B^*\xi \tag{III.62}$$

$$\tilde{A}_m = \sqrt{\mathcal{E}_m}A_m/\xi \tag{III.63}$$

we can then rewrite (III.60) in the form

$$\gamma_m(\tilde{B}) = \frac{\left|E\left[\tilde{B}^*\tilde{A}_m\right]\right|^2}{E\left[|\tilde{B}|^2\right] - \frac{1}{M}\sum_k \left|E\left[\tilde{B}^*\tilde{A}_k\right]\right|^2}. \tag{III.64}$$

Note that by symmetry, $\tilde{A}_1, \tilde{A}_2, \ldots, \tilde{A}_M$ are also zero-mean, mutually uncorrelated random variables, whose variances we denote by $\lambda_1, \lambda_2, \ldots, \lambda_M$.

Now, any $\tilde{B}$ with finite variance can be expanded in the form

$$\tilde{B} = \varepsilon + \sum_{k=1}^{M} \eta_k \tilde{A}_k \tag{III.65}$$

where, for all k, $E[\varepsilon^* A_k] = 0$ and η_k are complex constants. In particular, it suffices to choose

$$\eta_k = E\left[B^* \tilde{A}_k\right] / E\left[|\tilde{A}_k|^2\right].$$

Furthermore, from (II.58) we see that if $\hat{B}$ maximizes γ_m, so does $\kappa\hat{B}$ for any κ. Hence, to fix a particular solution, we may, without loss of generality, set $\eta_m = 1$.

Using (III.65), (III.64) simplifies to

$$\gamma_m(\tilde{B}) = \lambda_m^2 \left(E\left[|\varepsilon|^2\right] + \lambda_m(1 - \lambda_m/M) + \sum_{k \neq m} |\eta_k|^2 \lambda_k \left(1 - \lambda_k/M\right), \right)^{-1},$$

which, since

$$\lambda_i = E\left[\frac{\mathcal{E}_i |A_i|^2}{N_0 + \frac{1}{M}\sum_k \mathcal{E}_k |A_k|^2} \right] \leq M,$$

is maximized when $\varepsilon = 0$ and $\eta_k = 0$ for $k \neq m$. Thus, the maximum value of γ_m is obtained when B is of the form (II.59).

To obtain the bound (II.61), it suffices to substitute the optimum value of b into (III.60), which yields

$$\gamma_m/M = \frac{\varphi_m/M}{1 - \varphi_m/M} = \frac{1}{1 - \varphi_m/M} - 1$$

where

$$\varphi_m = E\left[\mathcal{E}_m |A_m|^2/\xi^2\right]$$

It therefore remains only to note that

$$1 - \varphi_m/M = E\left[\frac{\mathcal{N}_0\mathcal{W}_0 + \frac{1}{M}\sum_{k \neq m} \mathcal{E}_k |A_k|^2}{\mathcal{N}_0\mathcal{W}_0 + \frac{1}{M}\sum_k \mathcal{E}_k |A_k|^2} \right].$$

III.F Proof of Lemma 2

Let ξ_m denote the left hand side of (II.67). Then

$$\xi_1 = \xi_2 = \cdots = \xi_M \triangleq \xi_0$$

and, hence,

$$\begin{aligned}\xi_0 &= \frac{1}{M}E\left[\sum_k v_k\right] \\ &= \frac{1}{M}E\left[\frac{M+(M-1)\sum_k v_k}{1+\sum_k v_k}\right] \\ &= \frac{M-1}{M}+\frac{1}{M}\varphi \end{aligned} \tag{III.66}$$

where

$$\varphi = E\left[\frac{1}{1+\bar{\gamma}}\right] \tag{III.67}$$

with

$$\bar{\gamma} = \sum_k v_k. \tag{III.68}$$

Now $\bar{\gamma}$ as defined in (III.68) is an Erlang random variable of order M and mean M/μ. Hence,

$$\varphi = \int_0^\infty \frac{\mu^M \bar{\gamma}^{M-1} e^{-\mu\bar{\gamma}}}{(1+\bar{\gamma})\ (M-1)!}\, d\bar{\gamma}. \tag{III.69}$$

Exploiting the identities [15]

$$\int_0^\infty \frac{e^{-st}}{1+t}\, dt = e^s E_1(s)$$

$$\int_0^\infty t^k e^{-st}\, dt = k!/s^{k+1},$$

and

$$\frac{t^n}{t+1} = \frac{(-1)^n}{t+1} + \sum_{k=0}^{k-1}(-1)^{n-k-1}\, t^k$$

we get

$$\varphi = \frac{\mu^M}{(M-1)!}\left[(-1)^{M+1}e^\mu E_1(\mu) + \sum_{k=0}^{M-2}(-1)^{M-k}k!/\mu^{k+1}\right]. \tag{III.70}$$

Finally, substituting (III.70) into (III.66) we get (II.67).

■

Bibliography

[1] J. G. Proakis, *Digital Communications.* New York, NY: McGraw-Hill, second ed., 1989.

[2] W. C. Jakes, ed., *Microwave Mobile Communications.* New York, NY: John Wiley and Sons, 1974.

[3] G. D. Forney, Jr., "Burst-correcting codes for the classic bursty channel," *IEEE Trans. Commun.*, vol. COM-19, pp. 772–781, Oct. 1971.

[4] A. Wittneben, "An energy- and bandwidth-efficient data transmission system for time-selective fading channels," in *Proc. IEEE GLOBECOM*, 1990.

[5] S. Shamai (Shitz), L. H. Ozarow, and A. D. Wyner, "Information theoretic considerations for cellular mobile radio." Preprint., Jan. 1992.

[6] A. V. Oppenheim and R. W. Schafer, *Discrete-Time Signal Processing.* Englewood Cliffs, NJ: Prentice-Hall, 1989.

[7] M. J. E. Golay, "A class of finite binary sequences with alternate autocorrelation values equal to zero," *IEEE Trans. Inform. Theory*, vol. IT-18, no. 3, pp. 449–450, 1972.

[8] M. J. E. Golay, "The merit factor of long low-autocorrelation binary sequences," *IEEE Trans. Inform. Theory*, vol. IT-28, no. 3, pp. 543–549, 1982.

[9] G. F. M. Beenker, T. A. C. M. Claasen, and P. J. van Gerwen, "Design of smearing filters for data transmission," *IEEE Trans. Commun.*, vol. COM-33, pp. 955–963, Sept. 1985.

[10] K. Popat and K. Zeger, "Robust quantization of memoryless sources using dispersive FIR filters," *IEEE Trans. Commun.*, vol. 40, pp. 1670–1674, Nov. 1992.

[11] C. de Groot, D. Würtz, and K. H. Hoffmann, "Low autocorrelation binary sequences: Exact enumeration and optimization by evolutionary strategies," *Optimization*, vol. 23, pp. 369–384, 1992.

[12] D. V. Sarwate and M. B. Pursley, "Crosscorrelation properties of pseudorandom and related sequences," *Proc. IEEE*, vol. 68, pp. 593–619, May 1980.

[13] D. V. Sarwate, "Mean-square correlation of shift-register sequences," *IEE Proceedings, Part F*, vol. 131, pp. 101–106, Apr. 1984.

[14] E. A. Lee and D. G. Messerschmitt, *Digital Communication.* Boston, MA: Kluwer Academic, 1988.

[15] M. Abramowitz and I. A. Stegun, eds., *Handbook of Mathematical Functions.* New York, NY: Dover, 1965.

[16] W. C. Y. Lee, "Estimate of channel capacity in Rayleigh fading environment," *IEEE Trans. Vehic. Technol.*, vol. 39, pp. 187–189, Aug. 1990.

[17] T. M. Cover and J. A. Thomas, *Elements of Information Theory.* New York, NY: John Wiley and Sons, 1991.

[18] A. J. Viterbi, "Wireless digital communication: A view based on three lessons learned," *IEEE Commun. Mag.*, vol. 29, pp. 33–36, Sept. 1991.

[19] P. P. Vaidyanathan, *Multirate Systems and Filter Banks.* Englewood Cliffs, NJ: Prentice-Hall, 1993.

[20] H. L. Van Trees, *Detection, Estimation, and Modulation Theory, Part I.* New York, NY: John Wiley and Sons, 1968.

[21] L. R. Welch, "Lower bounds on the maximum cross correlation of signals," *IEEE Trans. Inform. Theory*, vol. IT-20, pp. 397–399, May 1974.

[22] M. J. E. Golay, "Multislit spectrometry," *J. Opt. Soc. Amer.*, vol. 39, pp. 437–444, 1949.

[23] M. J. E. Golay, "Static multislit spectrometry and its application to the panoramic display of infrared spectra," *J. Opt. Soc. Amer.*, vol. 41, pp. 468–472, 1951.

[24] M. J. E. Golay, "Complementary series," *IRE Trans. Inform. Theory*, vol. IT-7, pp. 82–87, Apr. 1961.

[25] S. Eliahou, M. Kervaire, and B. Saffari, "On Golay polynomial pairs," *Adv. Appl. Math.*, vol. 12, pp. 235–292, 1991.

[26] R. Turyn, "Ambiguity functions of complementary sequences," *IEEE Trans. Inform. Theory*, vol. IT-9, pp. 46–47, Jan. 1963.

[27] Y. Taki, H. Miyakawa, M. Hatori, and S. Namba, "Even-shift orthogonal sequences," *IEEE Trans. Inform. Theory*, vol. IT-15, pp. 295–300, Mar. 1969.

[28] C.-C. Tseng and C. L. Liu, "Complementary sets of sequences," *IEEE Trans. Inform. Theory*, vol. IT-18, pp. 644–652, Sept. 1972.

[29] H. S. Shapiro, "Extremal problems for polynomials and power series," Master's thesis, M. I. T., 1951.

[30] W. Rudin, "Some theorems on Fourier coefficients," *Proc. Amer. Math. Soc.*, vol. 10, pp. 855–859, 1959.

[31] A. M. Odlyzko, "Extremal and statistical properties of trigonometric polynomials with ± 1 and $0, 1$ coefficients." Preprint, 1993.

[32] D. J. Newman and J. S. Byrnes, "The L^4 norm of a polynomial with coefficients ± 1," *Amer. Math. Monthly*, vol. 97, pp. 42–45, 1990.

[33] S. Verdú, "Minimum probability of error for asynchronous Gaussian multiple-access channels," *IEEE Trans. Inform. Theory*, vol. IT-32, pp. 85–96, Jan. 1986.

[34] S. Verdú, "Optimum multiuser asymptotic efficiency," *IEEE Trans. Commun.*, vol. COM-34, pp. 890–897, Sept. 1986.